

11

5

Copy
RM L54L16

~~CONFIDENTIAL~~



RESEARCH MEMORANDUM

1111

STUDY OF SOME EFFECTS OF STRUCTURAL FLEXIBILITY ON THE
LONGITUDINAL MOTIONS AND LOADS AS OBTAINED FROM
FLIGHT MEASUREMENTS OF A SWEEP-WING BOMBER

By James J. Donegan and Carl R. Huss

Langley Aeronautical Laboratory
Langley Field, Va.

~~CLASSIFICATION CONTROLLED~~

UNCLASSIFIED

EXHIBIT COPY

*NACA Research
#RN-120*

*effective
Sept 13, 1957*

Authority of _____ Date _____

AMT 11-1-57

CLASSIFIED DOCUMENT

This material contains information affecting the National Defense of the United States within the meaning of the espionage laws, Title 18, U.S.C., Secs. 793 and 794, the transmission or revelation of which in any manner to an unauthorized person is prohibited by law.

NATIONAL ADVISORY COMMITTEE FOR AERONAUTICS

WASHINGTON

May 20, 1955

~~CONFIDENTIAL~~

NATIONAL ADVISORY COMMITTEE FOR AERONAUTICS

RESEARCH MEMORANDUM

STUDY OF SOME EFFECTS OF STRUCTURAL FLEXIBILITY ON THE
LONGITUDINAL MOTIONS AND LOADS AS OBTAINED FROM
FLIGHT MEASUREMENTS OF A SWEEP-WING BOMBER

By James J. Donegan and Carl R. Huss

SUMMARY

Some measurements obtained during elevator-pulse maneuvers with a Boeing B-47A airplane in the Mach number range from 0.62 to 0.82 are analyzed to obtain frequency responses in pitching velocity and normal load factor up to frequencies of 43 radians per second. Data-reduction methods are applied to these measurements to yield transfer coefficients and longitudinal stability derivatives.

The effects of structural flexibility are examined by considering the B-47A airplane configuration with three different amounts of flexibility and comparing the maximum responses of each to the same inputs. The "elastic" airplane contains all the flexibility characteristics of the B-47A as obtained from flight data, the "quasi-steady" airplane has the frequency response of the elastic airplane with the structural modes removed, and the "rigid" airplane has a frequency response with all effects of structural flexibility removed. Load factor and pitching velocities beyond the test range are calculated by mathematical extensions of the data to more hazardous conditions. Maximum time responses for the various airplanes subjected to triangular elevator pulses are then proportioned with one another to obtain quantitative measures of the effects of flexibility. The effects of including or omitting phasing between the various modes are also studied.

INTRODUCTION

In many investigations of the loads on relatively rigid airplanes, it is possible by means of a few well-chosen flight tests in a given speed range to obtain data which can be used to predict the loads which would

C

occur under more hazardous conditions. For instance, by proper analysis of the flight data, effective airplane parameters can be determined and the loads following much more severe control motions at any altitude can be predicted. References 1 and 2 are among several reports which present methods of reducing data to the required coefficient form.

Although the effects of small amounts of flexibility are handled by using the above methods and terming the reduced parameters as effective values, the effects of large amounts of flexibility, especially in combination with swept-wing configurations, cannot be bypassed in this manner. In such cases, structural modes and structural deformations which cause aerodynamic-center shifts and changes in aircraft frequency and damping became important variables. Usually these effects of additional structural modes on aircraft loads can be reasoned qualitatively but cannot be predicted numerically.

The investigations on loads currently being conducted by the National Advisory Committee for Aeronautics with the relatively flexible swept-wing Boeing B-47 airplane have one phase of the program devoted to obtaining data where the controls are pulsed in a fashion to excite the aircraft structural frequencies. This report is concerned with presenting an analysis of some of the elevator-pulse data obtained in the Mach number range from 0.62 to 0.82 as well as a reapplication of the results to more severe conditions.

Since the frequency plane is well adapted to analysis of structural modes, it has been used in this report to determine the dynamic characteristics of the Boeing B-47 airplane and to demonstrate the effects of these characteristics on the pitching velocity and incremental normal load factor. This type of analysis permits the simultaneous study of all the significant vibratory modes for the entire airplane.

SYMBOLS

b	airplane wing span, ft
\bar{c}	airplane mean aerodynamic chord, ft
C_L	airplane lift coefficient, L/qS
C_{L_α}	rate of change of airplane lift coefficient with angle of attack per radian
C_{L_δ}	rate of change of airplane lift coefficient with elevator deflection per radian

$C_{L\dot{\alpha}}$	rate of change of airplane lift coefficient with $\dot{\alpha}$ per radian per second
$C_{L\dot{\theta}}$	rate of change of airplane lift coefficient with pitching velocity per radian per second
C_m	pitching-moment coefficient of airplane, $M/qS\bar{c}$
$C_{m\alpha}$	rate of change of airplane pitching-moment coefficient with angle of attack per radian
$C_{m\delta}$	rate of change of airplane pitching-moment coefficient with elevator deflection per radian
$C_{m\dot{\theta}}$	rate of change of airplane pitching-moment coefficient with pitching velocity per radian per second
$C_{m\dot{\alpha}}$	rate of change of airplane pitching-moment coefficient with $\dot{\alpha}$ per radian per second
$\frac{\partial C_m}{\partial C_L}$	rate of change of airplane pitching-moment coefficient with lift coefficient
g	acceleration due to gravity, 32.2 ft/sec ²
H_p	pressure altitude, ft
I	airplane moment of inertia, slug-ft ²
$i = \sqrt{-1}$	
j	index of ω
k_y	airplane radius of gyration about pitching axis, ft
L	lift, lb
m	airplane mass, W/g , slugs
M	Mach number
Δn	incremental airplane load factor
q	dynamic pressure, $\frac{\rho v^2}{2}$, lb/ft ²

q_t	dynamic pressure in vicinity of horizontal tail, lb/ft ²
S	wing area, sq ft
S_t	horizontal-tail area, sq ft
t	time, sec
T	period, sec
V	true airspeed, ft/sec
V_e	equivalent airspeed, $V\sqrt{\frac{\rho}{\rho_0}}$, ft/sec
W	airplane weight, lb
x_t	length from center of gravity of airplane to aerodynamic center of tail (negative for conventional airplanes), ft
K_1, K_2, K_5, K_6 }	coefficients of transfer function relating $\dot{\theta}$ and δ_e (see appendix A)
α	wing angle of attack, radians
α_t	tail angle of attack, radians
$\dot{\alpha}$	rate of change of α with respect to time, radians/sec
γ_f	flight-path angle, radians
γ	dynamic response factor
θ	angle of pitch, $\alpha + \gamma_f$, radians
$\dot{\theta}$	pitching velocity, radians/sec
δ_e	elevator deflection, radians
ϵ	downwash angle, radians

$$\lambda = \frac{C_{m\dot{\alpha}}}{C_{m\dot{\theta}}}$$

η_t	tail efficiency factor, q_t/q
ρ	mass density of air, slugs/cu ft
ρ_0	mass density of air at sea level, slugs/cu ft
ξ	critical damping, percent
D	differential operator, d/dt
s	Laplace transform variable
ϕ	phase angle, deg or radians
ω	frequency, radians/sec
K_A	parameter defined in appendix A

Subscripts:

A	airplane
E	elastic
e	elevator
cg	center of gravity
F	flexible
i	input
n	natural
o	output
R	rigid
S	quasi-steady
t	tail
ϕ_0	phase angle at $\omega = 0$ radians/sec

Matrix notation:

$\left[\right]$ square matrix

$\left\{ \right\}$ column matrix

For sign conventions used see figure 1. Dots over a symbol refer to derivatives with respect to time, and a bar over a letter represents maximum value. The absolute value of any term is denoted by $||$.

AIRPLANE AND INSTRUMENTS

The airplane used in the tests was a Boeing B-47A airplane. A three-view drawing of the airplane is presented in figure 2 and pertinent dimensions are given in table I.

Because of the nature of the flight programs, it was necessary to install a large amount of instrumentation; however, only those instruments which were used to measure quantities pertinent to this paper will be mentioned in detail.

Linear accelerations were measured by standard NACA air-damped recording accelerometers and by remote-sensing oil-damped Statham electrical accelerometers in conjunction with oscillograph-type recording instruments. Angular velocities and angular accelerations were measured about the three airplane reference axes by rate-gyro-type electrically differentiating, magnetically damped standard NACA turnmeters. Control deflections were measured by remote-sensing electrical transmitters linked directly to the control surface in conjunction with a galvanometer. The angle of attack was measured by a flow-direction recorder having a vane-type sensing device located on a boom 73 inches ahead of the nose.

Electrical resistance-type wire strain gages were located throughout the structure. The output of these strain gages was recorded on oscillograph-type recorders. An NACA optigraph system for photographically measuring deflections was also incorporated into the instrumentation.

The data obtained from the instruments were recorded photographically. The recorders were synchronized at 0.1-second intervals by means of a common timing circuit. All instruments were damped to about 0.67 of critical damping. The location of the pertinent instruments or sensing elements is shown in figure 2. A summary of the quantities measured,

instrument locations, types of instrument, instrument accuracies, and natural frequencies is given in table II.

DATA-REDUCTION ERRORS

A detailed discussion of the factors affecting the accuracy of the Fourier method and frequency-response theory as applied to aircraft dynamic analyses is given in reference 3. This section, therefore, will be devoted to outlining briefly the main sources of error and the precautions taken to minimize the errors affecting this paper.

Two items which contribute the largest source of error in the data reduction are the reading accuracy and the reading time interval. In an effort to obtain maximum reading accuracy, time histories of the pertinent parameters were read on the universal telereader and telecorder in conjunction with an IBM card punch. With four-power magnification, the accuracy level of the reader is ± 0.003 inch of film deflection. The record sensitivities used and the accuracy levels (based on the reading accuracy for the primary data coordinates) that they signify are as follows:

	Record sensitivity	Accuracy level
$\dot{\theta}$	0.249 radians/sec/in.	± 0.00075 radian/sec
$\Delta\delta$	14 deg/in.	± 0.042 deg
Δn	1.013g/in.	$\pm 0.003g$

These reading errors will result in an error in the frequency-response amplitude ratio proportional to $1/\omega$ which is substantial only in the low-frequency range. Records were read at a reading interval $\Delta t = 0.02$ second. In order to have a minimum of six data points defining each full cycle, a reading interval of $\Delta t = 0.02$ second would permit a measured maximum frequency of

$$\bar{\omega} = \frac{2\pi}{6 \Delta t} = \frac{2\pi}{0.12} = 52.4 \text{ radians/sec}$$

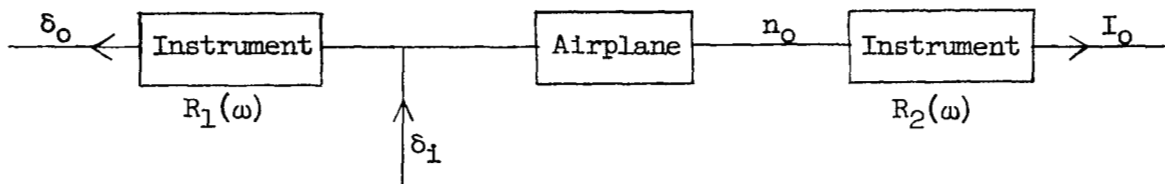
For a reading interval of $\Delta t = 0.02$ second, a rough estimate of the error in phase angle between the aircraft output and input for a given frequency (for example, $\omega = 43$ radians/sec) would be

$$\phi = \omega \Delta t = 43(0.02) = 0.86 \text{ radian} = 49^\circ$$

This is a substantial error in the phase angle for the highest frequency band, and its effect is treated elsewhere in the paper by considering the total effect of phasing.

In transforming a transient to the frequency plane by use of the Fourier method, one of the important factors which must be considered is frequency content of the input. The pulse method is desirable as a flight-test technique because it enables a frequency response to be computed from one flight run of a few seconds duration; however, it also has the limitation that the shape of the pulse input has an important effect on the harmonic content of the input. An input must have enough frequency content to excite sufficiently all harmonics over the considered frequency range in order to provide an accurate frequency response. As the triangular pulse approaches a pure impulse, the frequency content of the triangular pulse approaches the ideal frequency content; however, as the length of the base T_1 increases, this frequency content will bottom (approach zero-frequency content) at a frequency of approximately $\omega = 4\pi/T_1$. This condition produces an inaccurate frequency response at the bottoming frequencies. (It should be noted that bottoming is a characteristic of symmetrical inputs.) Thus, frequency content of the input must be examined carefully in order that sufficient excitation be provided over all the frequency range considered. As mentioned previously the pulse maneuvers used in this paper were selected in order to have good frequency content over the frequency range investigated.

Instrument errors are given in the section entitled "Airplane and Instruments." Corrections due to the dynamic response of instruments are made in the frequency plane after the harmonic analysis of the transient has been made.



In the usual open-loop diagram as shown above an elevator input δ_1 goes through a control position recorder and is recorded as δ_0 ; the same control input δ_1 results in the aircraft response n_0 which goes through an instrument and is recorded as I_0 . The apparent or measured frequency response without instrument corrections is then $\frac{I_0}{\delta_0}(i\omega)$. Now if $R_1(i\omega)$ is the frequency-response data of the control position instrument and $R_2(i\omega)$ the frequency-response data of the response recording instrument, then the desired aircraft frequency response $\frac{n_0}{\delta_1}(i\omega)$ is determined from the relation

$$\frac{n_o(i\omega)}{\delta_i} = \frac{I_o(i\omega)R_1(i\omega)}{\delta_o R_2(i\omega)}$$

If the natural frequencies of both of the recording instruments are close to each other, the amount of instrument correction to the frequency response is very small. An examination of table II indicates that this is the case for the instruments used on this aircraft.

From the foregoing discussion it is apparent the accuracy level of the results is least in the very low frequency bands (less than 0.75 radians/sec) in the very high frequency bands (above 40 radians/sec), and in the bands where the input frequency content tends to bottom.

METHODS

The term structural flexibility may have various interpretations depending upon the viewpoint. In this paper it refers to two separate phenomena, that of aircraft static aeroelastic deformations and that of deformations due to the structural or vibratory modes. References are frequently made and results given for the B-47A Boeing airplane with three separate amounts of flexibility: (1) an elastic or actual configuration with all its structural modes, (2) a quasi-steady configuration where response is affected only by quasi-steady aeroelastic effects such as would be measured in very slow maneuvers where higher vibratory modes are neglected, and (3) a rigid configuration whose characteristics are derived from the measured results. For the sake of brevity, these configurations are subsequently referred to as the elastic, quasi-steady, and rigid airplanes.

Selection of Tests

In this section, the methods used in selecting the flight runs for analysis and for reducing the results are outlined in a general way; additional details are given in the appendix.

The flight runs selected for detailed analyses were all short elevator-pulse maneuvers with the other controls held neutral. For these runs, the weight, altitude, and center-of-gravity position were nearly constant whereas the Mach number varied; however, some effects of altitude and center-of-gravity position on the aircraft short-period natural frequency were examined. Inasmuch as the effects of flexibility, transfer coefficients, and stability derivatives were all to be obtained from the data, use of the frequency plane was thought to be the most effective technique for evaluation of these quantities. As a result, only those

longitudinal maneuvers having elevator-pulse inputs of sufficiently high frequency content to excite as many of the aircraft symmetrical structural modes as possible were selected. Some typical time histories of the quantities used in the analyses of these maneuvers are given in figure 3 for three different Mach numbers.

Data Reduction

In order to obtain the frequency responses of the airplane, the time histories, such as given in figure 3, were transformed to the frequency plane by means of the Fourier method. The Fourier integrals of inputs and outputs were evaluated by using the IBM equipment and the method of integration of product curves described in reference 4. The frequency responses were obtained by taking the ratio of the Fourier integral of the output to the Fourier integral of the input as indicated by the expression

$$\frac{\Delta n}{\Delta \delta_e}(i\omega) = \frac{\int_0^{\infty} \Delta n(t) e^{-i\omega t} dt}{\int_0^{\infty} \Delta \delta_e(t) e^{-i\omega t} dt}$$

The frequency responses of the measured quantities $\left(\frac{\dot{\theta}}{\Delta \delta_e}\right)_{cg}$, $\left(\frac{\Delta n}{\Delta \delta_e}\right)_{cg}$, $\left(\frac{\Delta n}{\Delta \delta_e}\right)_{nose}$, $\left(\frac{\Delta n}{\Delta \delta_e}\right)_{wing\ tip}$, and $\left(\frac{\Delta n}{\Delta \delta_e}\right)_t$ thus obtained are shown in figure 4 for three different Mach numbers.

In this analysis, an attempt was made to extend the frequency range investigated as high as possible in order to get as many of the significant symmetrical vibratory modes as possible. In order to separate the short-period mode from the frequency-response curves of the pitching velocity, points were computed at every $\omega = 0.33$ radian per second up to 4 radians per second. Over the rest of the frequency range, points were measured at frequency intervals of $\Delta\omega = 1.3$ radians per second with additional fill-in points in the region of the structural modes. For the normal load-factor frequency-response curves the points were computed at frequency intervals of $\Delta\omega = 1.3$ radians per second with no fill-in points. In this case, the intervals may not be sufficiently small to define the short-period modes as well as the measured pitching velocities.

In figure 5 the predominant-symmetrical airplane frequencies are shown. The lines are the result of selecting the frequencies at which

the peak amplitude ratio in the Fourier analysis occurred. The test points were obtained from the results of a separate study of 100 runs involving 1700 traces in which the periods (in seconds) of all oscillations below 50 radians per second appearing on the records were converted to frequency and plotted against Mach number. The range of Mach number covered in this study was $0.43 \leq M \leq 0.84$; the range of center-of-gravity position was $0.12\bar{c}$ to $0.30\bar{c}$; and the range of altitude was 20,000 feet to 35,000 feet.

In figure 6 the natural frequency of the short-period mode is shown plotted against Mach number for various altitudes and center-of-gravity positions. The lines are arbitrarily drawn fairing lines through the data points.

Determination of Frequency Response of Rigid Configuration

In order to extrapolate results obtained from the flexible aircraft to those of the rigid aircraft, it was necessary to determine first the transfer coefficients and longitudinal stability derivatives of the flexible aircraft. The transfer coefficients in pitch were determined from the frequency-response data such as given in figure 4 by the vector-least-squares method of reference 5. In this analysis, the short-period regime of the frequency-response curve was fitted by this vector-least-squares method and the transfer coefficients shown by the test points in figure 7 were obtained. The solid lines through the data points for the plots of K_1 , K_2 , and K_5 against Mach number are arbitrarily drawn fairing lines. Inasmuch as the K_6 coefficient exhibited considerable scatter, the solid fairing line through the data was determined on the basis of the faired lines for the K_1 , K_2 , and K_5 coefficients and a value of C_{L_α} determined from flight measurements. These flight values of the lift-curve slope C_{L_α} are shown in figure 8 and were determined from an analysis of 25 runs obtained during slow push-pull maneuvers by plotting airplane lift coefficient C_L against angle of attack α .

The stability derivatives shown in the remainder of figure 8 were obtained from the selected flight data and are those normally associated with the short period of the flexible aircraft which includes static aeroelastic deformations. The computation of the derivatives of figure 8 was based on the equations of motion in the appendix, the values of λ from reference 6, and the aircraft mass and geometric parameters listed in table I. Also shown in figure 8 are the natural frequency and percent critical damping which were obtained from the transfer coefficients and the equations shown in the appendix.

In order to evaluate the effects of aeroelastic deformations on the Boeing B-47A airplane, the stability derivatives and transfer coefficients were modified for the rigid configuration. In this modification, the flexible-to-rigid parameters K_A , $(K_L)_R / (K_L)_F$, and $\Delta \left(\frac{\partial C_m}{\partial C_{L,A}} \right)$ shown in figure 9 were taken from reference 7 and are based on tests of models having various degrees of stiffness. The parameter $\left(\frac{\partial C_m}{\partial \delta_e} \right)_R / \left(\frac{\partial C_m}{\partial \delta_e} \right)_F$ was taken from reference 8. These parameters of figure 9 are for a gross weight of 125,000 pounds and have negligible variation for the range of gross weight in this paper. These parameters were determined on the basis of changes in the spanwise lift distribution, a shift in the aerodynamic center, changes in the tail angle of incidence, changes in control effectiveness, and so forth which were caused by static deformations of the aircraft structure due to flexibility in a swept-wing configuration. The parameters of figure 9 in conjunction with the relations contained in the appendix were used to compute the stability derivatives and transfer coefficients of the rigid airplane. The stability derivatives of the rigid configuration and transfer coefficients thus computed are indicated in figures 7 and 8 by broken lines.

The frequency response in pitching velocity for the rigid airplane shown in figure 10 was then computed by using the rigid transfer coefficients and frequency-response relations given in the appendix. Also shown in figure 10 are the frequency responses in pitching velocity for the elastic airplane and quasi-steady airplane. The frequency response of the elastic airplane was shown previously in figure 4 and was computed directly from the measured flight data. The frequency response of the quasi-steady airplane is the short-period mode of the elastic airplane with the structural modes removed.

DYNAMIC-RESPONSE ANALYSIS

Most of the figures presented thus far have dealt with data and parameters extracted from the data as obtained from the flight-test maneuvers. In order to study more fully the effects of flexibility on the loads and longitudinal responses of the aircraft, however, further computation with these parameters and the extension of the data to more hazardous conditions are required. The response characteristics of the elastic aircraft used in combination with a severe but practical type of control input permit extension of the data beyond the test range.

The triangular pulse method used in reference 9 in a study of the maximum dynamic loads during landing appeared to be the most appropriate

type of input and was selected on the basis of several desirable features: The frequency content of the triangles could easily be varied by changing the time base T_1 of the triangle; the triangles had sufficient frequency content to excite the higher airplane vibratory modes; and the triangular input was well adapted to synthesizer operation and loads computations. The triangles used in this investigation were isosceles.

In some of the computations of response to triangular inputs, the electromechanical Fourier synthesizer was used to produce transient-response curves from frequency-response data. In other cases the computation was carried out on calculating machines. The operation of the Fourier synthesizer is described in some detail in reference 4.

Figure 11 shows three computed time histories of the response in pitching velocity of the elastic, quasi-steady, and rigid airplanes to a triangular input. In this case, the results are shown for a period ratio of $T_1/T = 0.1$ and a Mach number of 0.82. In the computations of figures 11 to 20, the maximum elevator deflection is 0.1 radian.

By varying the ratio T_1/T of the input over a range of values, a series of plots similar to those of figure 11 were obtained. The maximum value of pitching velocity of the elastic airplane following the triangular pulse was designated as $\bar{\theta}_E$, of the quasi-steady airplane as $\bar{\theta}_S$, and of the rigid airplane as $\bar{\theta}_R$. A comparison of these maximum transient responses was then made by plotting their ratios against the period ratio T_1/T as shown in figure 12. The ratio $\bar{\theta}_S/\bar{\theta}_R$ indicates the effect of static aeroelastic deformation, the ratio $\bar{\theta}_E/\bar{\theta}_S$ indicates the effect of the structural modes, and the ratio $\bar{\theta}_E/\bar{\theta}_R$ indicates the overall effects of flexibility on the longitudinal response in pitching velocity of the airplane.

The data of figure 13 are a conversion of the ratios of figure 12 to a percent alleviation or magnification factor of the pitching velocity. The ordinate is constructed so that positive values indicate alleviation and negative values indicate magnification.

Plots similar to those of figure 11 were also obtained for the load factor at the center of gravity. A plot of the ratios of maximum load factor similar to those of maximum pitching velocity of figure 12 was obtained and is presented in figure 14. The same trend in normal load factor as in pitching velocity is indicated. As noted previously, the ratio $\Delta n_S/\Delta n_R$ indicates the effects of static aeroelastic deformation;

the ratio $\overline{\Delta n_E} / \overline{\Delta n_S}$ indicates the effect of structural modes; and the ratio $\overline{\Delta n_E} / \overline{\Delta n_R}$ indicates the overall effects of flexibility on the normal load-factor response.

Another of the effects of flexibility obtained from figure 11 is the change in the time to reach peak pitching velocity for the elastic, quasi-steady, and rigid airplanes. Figure 15 is a plot of the time to reach peak pitching velocity against the period ratio T_1/T for the three airplanes.

A similar plot of time to reach peak load factor at the center of gravity against the period ratio T_1/T for the elastic, quasi-steady, and rigid airplane is shown in figure 16.

In the study of flexibility it is of interest to assess the importance of the phasing relation between the modes. Up to this point, all results have included phasing but, in order to study the importance of this phase relation, the calculations were repeated with phasing removed and the results compared with the previous computations. Phasing was removed from the computation by considering the phase angle of the airplane as constant and equal to the value of $\omega = 0$ over the entire frequency range. The ratio of maximum pitching velocity, not including phasing, to the maximum pitching velocity, including phasing, plotted against the period ratio is shown in figure 17; whereas, figure 18 is a similar plot for maximum incremental normal load factor at the center of gravity. Inasmuch as considerable errors can occur in the phase-angle computation in the high-frequency range of the spectrum, these comparisons also aid in determining the effects of such errors on the maximum loads and longitudinal responses.

Another important parameter in the study of loads associated with flexible structures is the dynamic-response factor (see ref. 9) defined as $\gamma = \frac{\Delta n_{dyn}}{\Delta n_{static}}$ where Δn_{dyn} refers to the maximum amplitude of incremental load factor and Δn_{static} refers to the steady-state amplitude of the incremental load factor for the same input. The variation of the dynamic response factor γ is shown in figure 19 plotted against the period ratio T_1/T for the elastic, quasi-steady, and rigid airplanes at a Mach number of 0.82 and for the elastic and quasi-steady airplanes at a Mach number of 0.66.

In order to obtain an overall picture of the deformations and vibrations taking place in a typical flight maneuver, a three-dimensional plot of the time histories of the wing and fuselage bending deformations during

a pulse maneuver is shown in figure 20. This is the same maneuver as shown in figures 3(a) and 4(a).

DISCUSSION

The methods employed in this paper are all based on the assumptions of linearity and the small perturbation theory. The flight-test technique of pulsing the elevator is essentially a small-perturbation method. Inasmuch as the flight conditions and maneuvers analyzed were selected so that the airplane would respond in the linear range of the transfer coefficients and stability derivatives, the quantities obtained from this analysis apply most accurately to this linear range.

The frequency-response curves shown in figure 4 indicate the dynamic characteristics of the elastic airplane such as the short-period mode and the vibratory or structural modes which appear as peaks on the amplitude-ratio curves. Evidences of the airplane phugoid mode do not appear as is to be expected because the phugoid is a long-period mode which cannot be detected from the data with pulse-type inputs. In general, a measure of the relative importance of each of the individual modes on the response of the airplane is given by the resonant amplitude of the modes and by the frequency at which the modes occur. The higher the frequency at which the mode occurs, the less effect the mode will have in the normal airplane maneuver range since any practical pilot-applied forcing function will excite higher harmonics with lower amplitude. The structural mode at $\omega = 27.5$ radians per second appears as a dominant mode in all the frequency-response traces; this is also particularly noticeable in the three-dimensional plot of airplane deflections shown in figure 20.

The plot of symmetrical airplane frequencies shown in figure 5 indicates an increase in the natural frequency of the short-period mode with increasing Mach number and, as expected, little or no change with Mach number of the structural mode frequencies. Mach number, however, has a definite effect on resonant amplitudes of the structural modes and generally shows an increase in amplitude with increasing Mach number. An attempt was made to identify the structural frequencies in figure 5 with the usual uncoupled cantilevered modes. This attempt proved unsuccessful inasmuch as the airplane vibratory modes are coupled modes containing elastic and aerodynamic coupling and, because this is a swept-wing configuration, each wing bending mode has its own associated torsion.

In figure 6 the effects of either a rearward movement of the center-of-gravity position or an increase in altitude is seen to decrease the natural frequency of the short-period mode in accordance with expectations.

The effects of static aeroelastic deformations in the airplane transfer coefficients and stability derivatives are indicated in figures 7 and 8 by the difference between the solid and broken lines. The force derivatives C_{L_α} and transfer coefficients for the flexible airplane are shown to be less than those for the rigid airplane. The elevator effectiveness derivative $C_{m\delta}$ is reduced because of flexibility. The largest effect due to flexibility is evidenced in the C_{m_α} derivative.

From the curves of short-period natural frequency ω_n and percent critical damping ξ shown in figure 8 for the flexible and rigid airplanes it is evident that flexibility reduces the short-period natural frequency and increases ξ . The reduction in ω_n appears to be due to the reduction in C_{M_α} .

The frequency responses shown in figure 10 for the three different amounts of flexibility in the airplane show that, as elasticity is introduced into the rigid structure, a change takes place in the frequency response as evidenced not only by the change in the short-period mode but also by the appearance of vibratory modes.

In the typical time responses of the elastic, quasi-steady, and rigid airplane shown in figure 11, the main change in the time response of an airplane for three separate amounts of flexibility is seen to cause the elastic-airplane response to oscillate around the quasi-steady-airplane response and to modify the maximum amplitudes of the responses and times to peak amplitude for each case.

Some pulses applied to the airplane imposed more severe rates of elevator displacement than could be achieved by a pilot in flight. An analysis of the pulse maneuvers of the flight-test program indicated a maximum elevator rate of 0.75 radian per second which is equivalent to $T_1 = 0.27$ second for a 0.1-radian deflection. For the calculations presented in this paper, this value represents a period ratio $T_1/T = 0.1$ which is the minimum that the pilot can apply to the airplane by control inputs. Under unusual conditions, however, when the forcing function is attributable to gusts or separation phenomena, smaller period ratios may be attained. In this lower range, however, the computed values may be high because unsteady lift effects were not considered in the calculations.

The ratio $\bar{\theta}_S/\bar{\theta}_R$ in figure 12 indicates that static aeroelastic deformation in all cases reduces the maximum airplane response in pitching velocity. The ratio $\bar{\theta}_E/\bar{\theta}_S$ indicates an increase in maximum pitching

velocity over the low ranges of T_1/T where the structural modes are excited and indicates no effect over the high ranges of T_1/T where there is insufficient frequency content in the input to excite the structural modes. The ratio $\bar{\theta}_E/\bar{\theta}_R$ indicates the overall effects of flexibility on pitching-velocity response. Because of the excitation of the structural modes in the lower range of T_1/T , the maximum response in pitching velocity is increased. In the higher range of T_1/T where the structural modes are not excited, static aeroelastic deformation decreases the maximum airplane response in pitching velocity.

The results given in figure 13 show that static aeroelastic deformation provides approximately 11-percent alleviation over the rigid case, and the structural modes provide magnification of the response up to 90 percent.

The ratios of maximum incremental load-factor values at the center of gravity shown in figure 14 indicate the same trends as the maximum pitching-velocity responses, that is, an alleviation due to static aeroelastic deformation and a magnification due to the structural modes when excited.

The time to reach peak pitching velocity as shown in figure 15 is a minimum for the rigid airplane and a maximum for the quasi-steady airplane; the time for the elastic airplane varies between the two limits. The effect of static aeroelastic deformation is therefore one of increasing the time to reach peak pitching velocity over the rigid case; whereas, the effect of the structural modes is to decrease the time to reach peak pitching velocity over the quasi-steady airplane.

The effects of the structural frequencies on the time-to-peak-load factor is shown in figure 16 to be a decrease in the time-to-peak-load factor when the structural frequencies are excited.

The effect of removing the phase-angle relation in the computations as shown in figure 17 is to increase the maximum pitching-velocity response in all cases. This is in accordance with expectations inasmuch as, in a simple vibratory system, the effect of removing the phase-angle relation is equivalent to removing damping from the system.

The effect of excluding the phase-angle relation from the computation of maximum load factor at the center of gravity as shown in figure 18 indicates the same trend as for the case of maximum pitching-velocity response, namely, to increase the maximum load factor in all cases.

The dynamic response factor γ_S of the quasi-steady airplane is approximately 1.2 for a Mach number of 0.82 and 1.3 for a Mach number

of 0.66. (See fig. 19.) The curve for dynamic response factor γ_E against the period ratio T_1/T for the elastic airplane exhibits two definite peaks, one due to the structural modes and the other due to the short-period mode. The maximum dynamic overshoot of the elastic airplane, however, is the same as the quasi-steady-airplane dynamic overshoot. It should be noted that, if the short-period natural frequency and vibratory-mode frequencies were closer together, then the dynamic response of the short-period mode and vibratory modes could add and form a critical loading condition. (The dynamic response factor γ_R for the rigid airplane is approximately 1.43 for a Mach number of 0.82.) The overall Mach number effect appears to be a decrease in dynamic response factor γ with increasing Mach number due in part to an increase in Δn_{static} with Mach number.

The three-dimensional time histories of wing and fuselage deformations shown in figure 20 indicate that all the modes are coupled. The fuselage deformations can be seen to be the superposition of the vibratory modes on the static aeroelastic deformation.

CONCLUSIONS

Effects of structural flexibility have been examined by considering the swept-wing Boeing B-47A airplane with three different amounts of flexibility and comparing the maximum responses of each to the same inputs. The analysis of some of the elevator-pulse data of this paper apply specifically in the Mach number range from 0.62 to 0.82 in the linear range of longitudinal response, and the following conclusions are established:

1. Static aeroelastic deformation alleviates loads and decreases the maximum pitching-velocity response.
2. The structural modes when excited increase loads and maximum pitching-velocity response.
3. The magnitude of the force derivative $C_{L\alpha}$, two moment derivatives $C_{m\alpha}$ and $C_{m\delta}$, and the transfer coefficients are less for the "quasi-steady" airplane than for the "rigid" airplane.
4. The short-period natural frequency of the "elastic," "quasi-steady," and "rigid" airplane decreases with increasing altitude, with rearward movement of the center of gravity, and with decreasing Mach number.

5. The structural frequencies of the "elastic" airplane show little change with Mach number or altitude.
6. The "quasi-steady" airplane has a lower natural short-period frequency ω_n and a somewhat higher percent critical damping ξ than the "rigid" airplane.
7. The inclusion of phasing in the computation of longitudinal coordinate responses and loads of the airplane reduces the maximum values.
8. The time-to-peak-pitching-velocity response and incremental load-factor response of the "quasi-steady" airplane is higher than that for the "rigid" airplane or the "elastic" airplane when the structural modes are excited.
9. Airplane structural frequencies should be well separated from the short-period mode and should be sufficiently high to be beyond the pilot's ability to excite them with control inputs.

Langley Aeronautical Laboratory,
National Advisory Committee for Aeronautics,
Langley Field, Va., December 8, 1954.

APPENDIX

SUMMARY OF MATHEMATICAL RELATIONS USED IN EVALUATING DATA

The longitudinal equations of motion for horizontal flight used in this analysis (see ref. 2) are

$$\frac{W}{qS} \Delta n = C_{L\alpha} \Delta\alpha + C_{L\delta} \Delta\delta_e \quad (A1)$$

$$\frac{I}{qS\bar{c}} \ddot{\theta} = C_{m\alpha} \Delta\alpha + C_{m\dot{\alpha}} \dot{\alpha} + C_{m\dot{\theta}} \dot{\theta} + C_{m\delta} \Delta\delta_e \quad (A2)$$

and

$$\dot{\theta} = \dot{\alpha} + \dot{\gamma}_f = \dot{\alpha} + \frac{g}{V} \Delta n \quad (A3)$$

These equations are based on the usual assumptions of linearity, small angles, and no loss in airspeed during the maneuver.

The usual transfer function between pitching velocity and incremental elevator deflection obtained by solving equations (A1) to (A3) simultaneously is given by

$$D^2\dot{\theta} + K_1 D\dot{\theta} + K_2 \dot{\theta} = K_5 D\delta_e + K_6 \delta_e \quad (A4)$$

where the transfer coefficients K_1 , K_2 , K_5 , and K_6 are defined as follows:

$$K_1 = \frac{qS}{V} \left[\frac{C_{L\alpha}}{m} - \frac{\bar{c}V}{I} (C_{m\dot{\alpha}} + C_{m\dot{\theta}}) \right] \quad (A5)$$

$$K_2 = - \frac{qS\bar{c}}{I} \left(C_{m\alpha} + C_{m\dot{\theta}} \frac{C_{L\alpha} qS}{mV} \right) \quad (A6)$$

$$K_5 = \frac{qS\bar{c}}{I} \left(C_{m\delta} - \frac{qS}{mV} C_{L\delta} C_{m\dot{\alpha}} \right) \quad (A7)$$

$$K_6 = \frac{qS\bar{c}}{I} \frac{qS}{mV} (C_{L_\alpha} C_{m_\delta} - C_{L_\delta} C_{m_\alpha}) \tag{A8}$$

The pitching-velocity transfer coefficients K_1 , K_2 , K_5 , and K_6 of equation (A4) were computed from the pitching-velocity frequency-response data by use of the vector-least-squares method of reference 5 as follows:

$$\begin{Bmatrix} K_6 \\ K_5 \\ K_1 \\ K_2 \end{Bmatrix} = \begin{bmatrix} N & 0 & \sum_{j=\omega_1}^{\omega_n} (\omega B_{\dot{\theta}})_j & \sum_{j=\omega_1}^{\omega_n} (-A_{\dot{\theta}})_j \\ 0 & \sum_{j=\omega_1}^{\omega_n} (\omega)^2_j & \sum_{j=\omega_1}^{\omega_n} (-\omega^2 A_{\dot{\theta}})_j & \sum_{j=\omega_1}^{\omega_n} (-\omega B_{\dot{\theta}})_j \\ \sum_{j=\omega_1}^{\omega_n} (\omega B_{\dot{\theta}})_j & \sum_{j=\omega_1}^{\omega_n} (-\omega^2 A_{\dot{\theta}})_j & \sum_{j=\omega_1}^{\omega_n} (\omega^2 \left| \frac{\dot{\theta}}{\delta} \right|^2)_j & 0 \\ \sum_{j=\omega_1}^{\omega_n} (-A_{\dot{\theta}})_j & \sum_{j=\omega_1}^{\omega_n} (-\omega B_{\dot{\theta}})_j & 0 & \sum_{j=\omega_1}^{\omega_n} \left(\left| \frac{\dot{\theta}}{\delta} \right|^2 \right)_j \end{bmatrix}^{-1} \begin{Bmatrix} \sum_{j=\omega_1}^{\omega_n} (-\omega^2 A_{\dot{\theta}})_j \\ \sum_{j=\omega_1}^{\omega_n} (-\omega^3 B_{\dot{\theta}})_j \\ 0 \\ \sum_{j=\omega_1}^{\omega_n} (\omega^2 \left| \frac{\dot{\theta}}{\delta} \right|^2)_j \end{Bmatrix} \tag{A9}$$

where

$$A_{\dot{\theta}} = \left| \frac{\dot{\theta}}{\delta} \right| \cos \Phi_{\dot{\theta}\delta} \tag{A10}$$

$$B_{\dot{\theta}} = \left| \frac{\dot{\theta}}{\delta} \right| \sin \Phi_{\dot{\theta}\delta} \tag{A11}$$

and N is the number of data points used.

The following expressions and procedures were used in the determination of stability derivatives. The C_{L_α} derivative, as mentioned in the text, was determined from a separate investigation of slow push-pull maneuvers. Values of the ratio λ used in this report were obtained from reference 9. The remaining longitudinal derivatives were computed by use of the following approximate relations from reference 2:

$$\left(C_{m\dot{\theta}} + C_{m\dot{\alpha}} \right) = \frac{I}{qS\bar{c}} \frac{qS}{mV} \left(C_{L\alpha} - \frac{mV}{qS} K_1 \right) \quad (A12)$$

$$C_{m\dot{\alpha}} = \lambda C_{m\dot{\theta}} \quad (A13)$$

$$C_{m\alpha} = -\frac{I}{qS\bar{c}} K_2 - C_{L\alpha} \frac{qS}{mV} C_{m\dot{\theta}} \quad (A14)$$

$$C_{m\delta} = \frac{I}{qS\bar{c}} \frac{K_5}{1 - \frac{qS}{mV} \frac{\bar{c}}{x_t} \lambda C_{m\dot{\theta}}} \quad (A15)$$

$$C_{L\delta} = \frac{\bar{c}}{x_t} C_{m\delta} \quad (A16)$$

$$\omega_n = \sqrt{K_2} \quad (A17)$$

$$\xi = \frac{K_1}{2\omega_n} \quad (A18)$$

In converting the rigid stability derivatives from the derivatives of the flexible airplane, the following definitions and expressions were used:

$$\left(C_{L\alpha} \right)_R = K_A \left(C_{L\alpha} \right)_F \quad (A19)$$

$$\left(K_1 \right)_R = \frac{\left(K_1 \right)_R}{\left(K_1 \right)_F} \left(K_1 \right)_F \quad (A20)$$

$$\left(C_{m\delta} \right)_R = \frac{\left(\frac{\partial C_m}{\partial \delta} \right)_R}{\left(\frac{\partial C_m}{\partial \delta} \right)_F} \left(\frac{\partial C_m}{\partial \delta} \right)_F \quad (A21)$$

$$\left(\frac{\partial C_m}{\partial C_L}\right)_R = \left(\frac{\partial C_m}{\partial C_L}\right)_F - \Delta \left(\frac{\partial C_m}{\partial C_L}\right) \quad (A22)$$

$$(C_{m\alpha})_R = (C_{L\alpha})_R \left(\frac{\partial C_m}{\partial C_L}\right)_R \quad (A23)$$

Frequency response for the rigid airplane in pitching velocity was computed by using the following relations for amplitude ratio and phase angle:

$$\left|\frac{\dot{\theta}}{\delta_e}\right| = \sqrt{\frac{K_6^2 + (K_5\omega)^2}{(K_2 - \omega^2)^2 + (K_1\omega)^2}} \quad (A24)$$

$$\phi_{\dot{\theta}/\delta_e} = \tan^{-1} \frac{K_5\omega}{K_6} - \tan^{-1} \frac{K_1\omega}{K_2 - \omega^2} \quad (A25)$$

REFERENCES

1. Donegan, James J., and Pearson, Henry A.: Matrix Method of Determining the Longitudinal-Stability Coefficients and Frequency Response of an Aircraft From Transient Flight Data. NACA Rep. 1070, 1952. (Supersedes NACA TN 2370.)
2. Donegan, James J.: Matrix Methods for Determining the Longitudinal-Stability Derivatives of an Airplane From Transient Flight Data. NACA Rep. 1169, 1954. (Supersedes NACA TN 2902.)
3. Breaux, G. P., and Zeiller, E. L.: Dynamic Response Program on the B-36 Airplane: Part III - Presentation and Theoretical Considerations of the Transient Analysis Method Employed for Obtaining Frequency Response Functions From Flight Data. Rep. No. FZA-36-195, Consolidated Vultee Aircraft Corp., Feb. 14, 1952.
4. Eggleston, John M., and Mathews, Charles W.: Application of Several Methods for Determining Transfer Functions and Frequency Response of Aircraft From Flight Data. NACA TN 2997, 1953.
5. Schumacher, Lloyd E.: A Method for Evaluating Aircraft Stability Parameters From Flight Test Data. USAF Tech. Rep. No. WADC-TR-52-71, Wright Air Dev. Center, U. S. Air Force, June 1952.
6. Cole, Henry A., Jr., Brown, Stuart C., and Holleman, Euclid C.: Experimental and Predicted Longitudinal Response Characteristics of a Large Flexible 35° Swept-Wing Airplane at an Altitude of 35,000 Feet. NACA RM A54H09, 1954.
7. Budish, Nathan N.: Longitudinal Stability at High Airspeeds. Rep. No. D-8603-0 (Contract No. W33-038 ac-22413), Boeing Aircraft Co., Feb. 29, 1952.
8. Skoog, Richard B.: An Analysis of the Effects of Aeroelasticity on Static Longitudinal Stability and Control of a Sweptback-Wing Airplane. NACA RM A51C19, 1951.
9. Biot, M. A., and Bisplinghoff, R. L.: Dynamic Loads on Airplane Structures During Landing. NACA WR W-92, 1944. (Formerly NACA ARR 4H10.)

TABLE I.- PERTINENT PHYSICAL CHARACTERISTICS AND

DIMENSIONS OF BOEING B-47A TEST AIRPLANE

Total wing area, sq ft	1,428
Wing span, ft	116
Wing aspect ratio	9.43
Wing thickness ratio, percent	12
Wing taper ratio	0.42
Wing mean aerodynamic chord, in.	155.9
Wing sweepback (25-percent chord line), deg	35
Total horizontal-tail area, sq ft	268
Horizontal-tail span, ft	33
Horizontal-tail mean aerodynamic chord, in.	102.9
Horizontal-tail sweepback (25-percent chord line), deg	35
Distance from center of gravity to quarter chord of horizontal-tail MAC (center of gravity at $0.21\bar{c}$), ft	47
Airplane weight, lb	125,000 to 127,000
Airplane pitching radius of gyration, k_y , ft	19.5
λ	0.18

TABLE II.- SUMMARY OF INSTRUMENTATION AND ACCURACIES

Quantity measured	Where measured	Instrument used	Units	Instrument range	Instrument accuracy	Natural frequency, radians/sec
Normal acceleration	Center of gravity	Three-component air-damped accelerometer	g	-1 to 4	0.0125	66
	Tail	-----do-----	g	-2 to 6	0.0200	66
	Optigraph housing	Two-component air-damped accelerometer	g	-1 to 4	0.0125	66
	10 wing stations	Statham electrical accelerometer and galvanometer	g	±12 at tip to 5.05 at inboard station -4.25	Recording 0.1	Accelerometer 628 Recorder 75
	6 fuselage stations	-----do-----	g	7.34 to 5.8 -2.51 -7.8	-----do-----	Do.
Pitching velocity	Center of gravity	Angular velocity recorder	$\frac{\text{radians}}{\text{sec}}$	±0.25	0.005	85
Pitching acceleration	Center of gravity	Angular acceleration recorder	$\frac{\text{radians}}{\text{sec}^2}$	±0.50	0.010	44
Elevator angle	Midelevator semispan	Control position transmitter and galvanometer	deg	25 up and 15 down	0.40	75
Angle of attack	73 inches in front of nose	Vane-type transmitter of flow-direction recorder	deg	±30	0.10	94
Periods of various structural frequencies	Several wing and fuselage locations	Strain gages and accelerometers	sec	Varied	-----	75
Time	-----	Timer	sec	-----	Approximately 0.005	-----

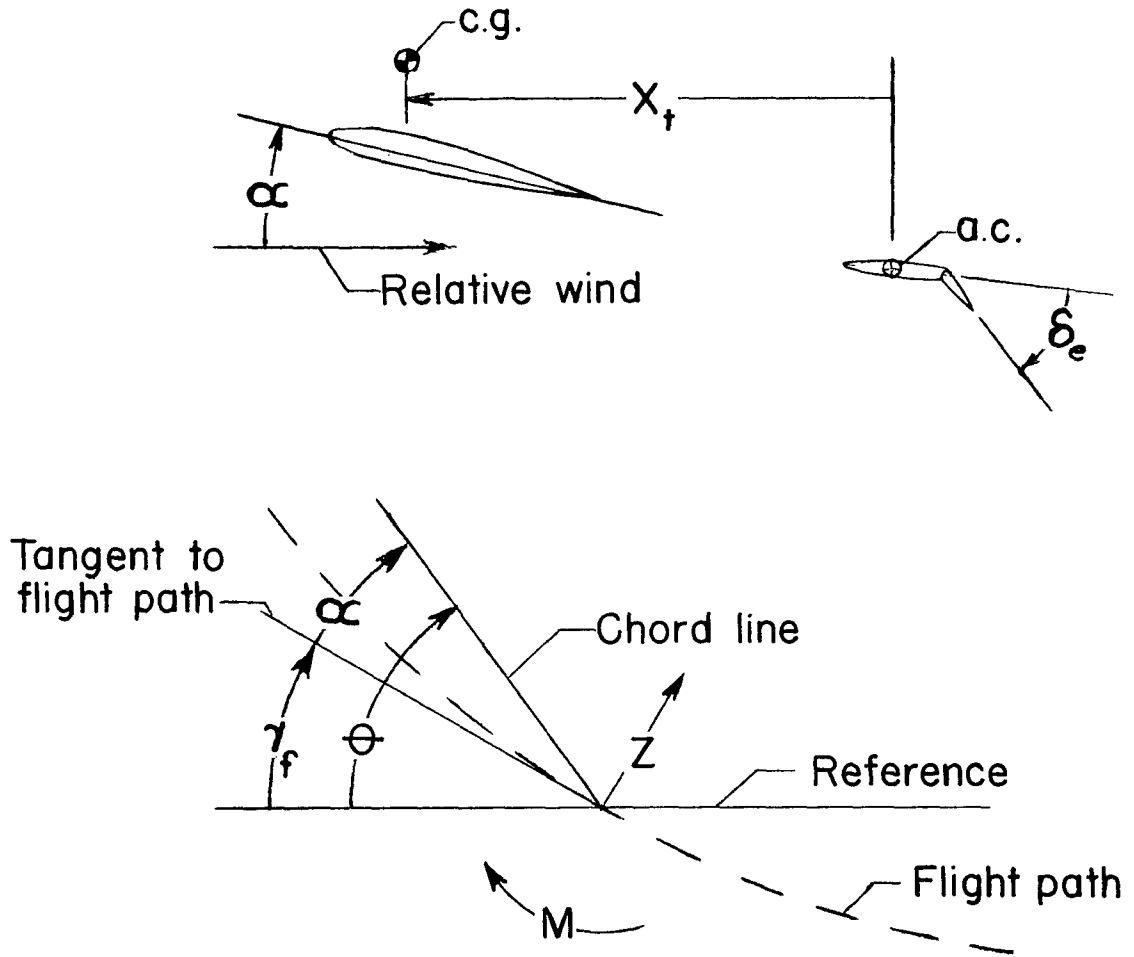


Figure 1.- Sign convention employed with positive directions shown.

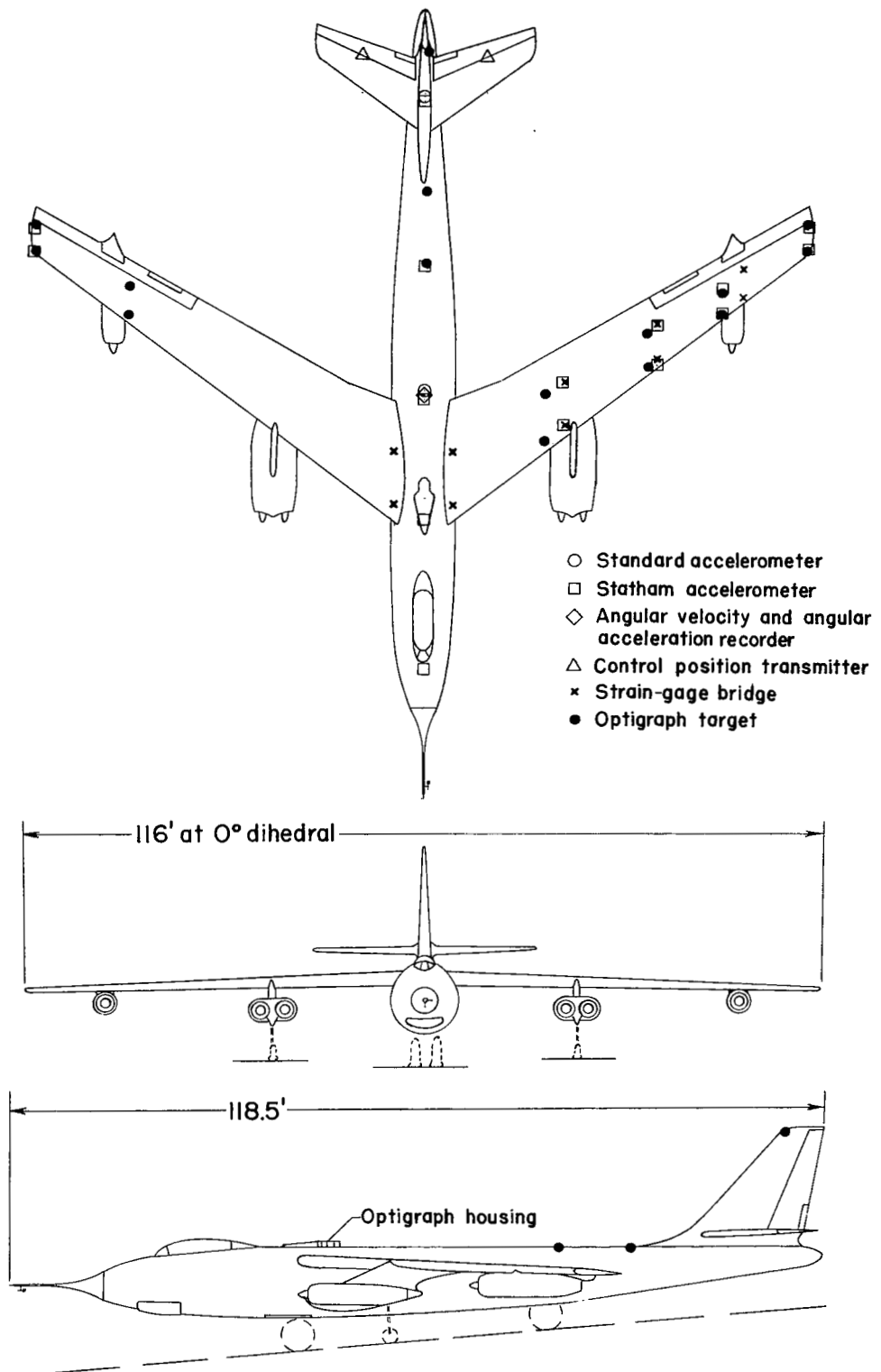
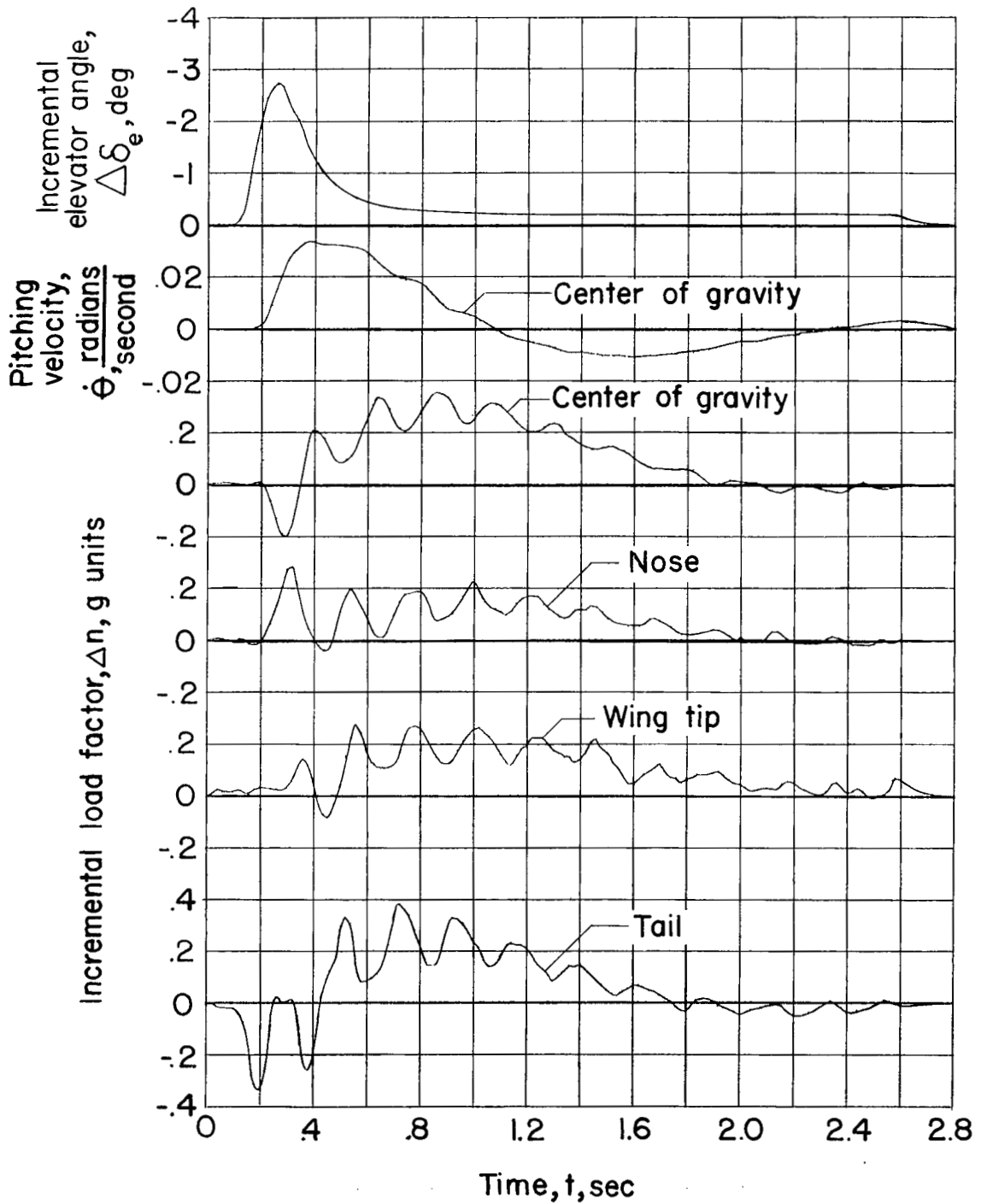


Figure 2.- Three-view drawing of test airplane.



(a) $M = 0.82$.

Figure 3.- Time histories of measured quantities. $H_p = 30,000$ feet; center-of-gravity position at $0.21\bar{l}$.

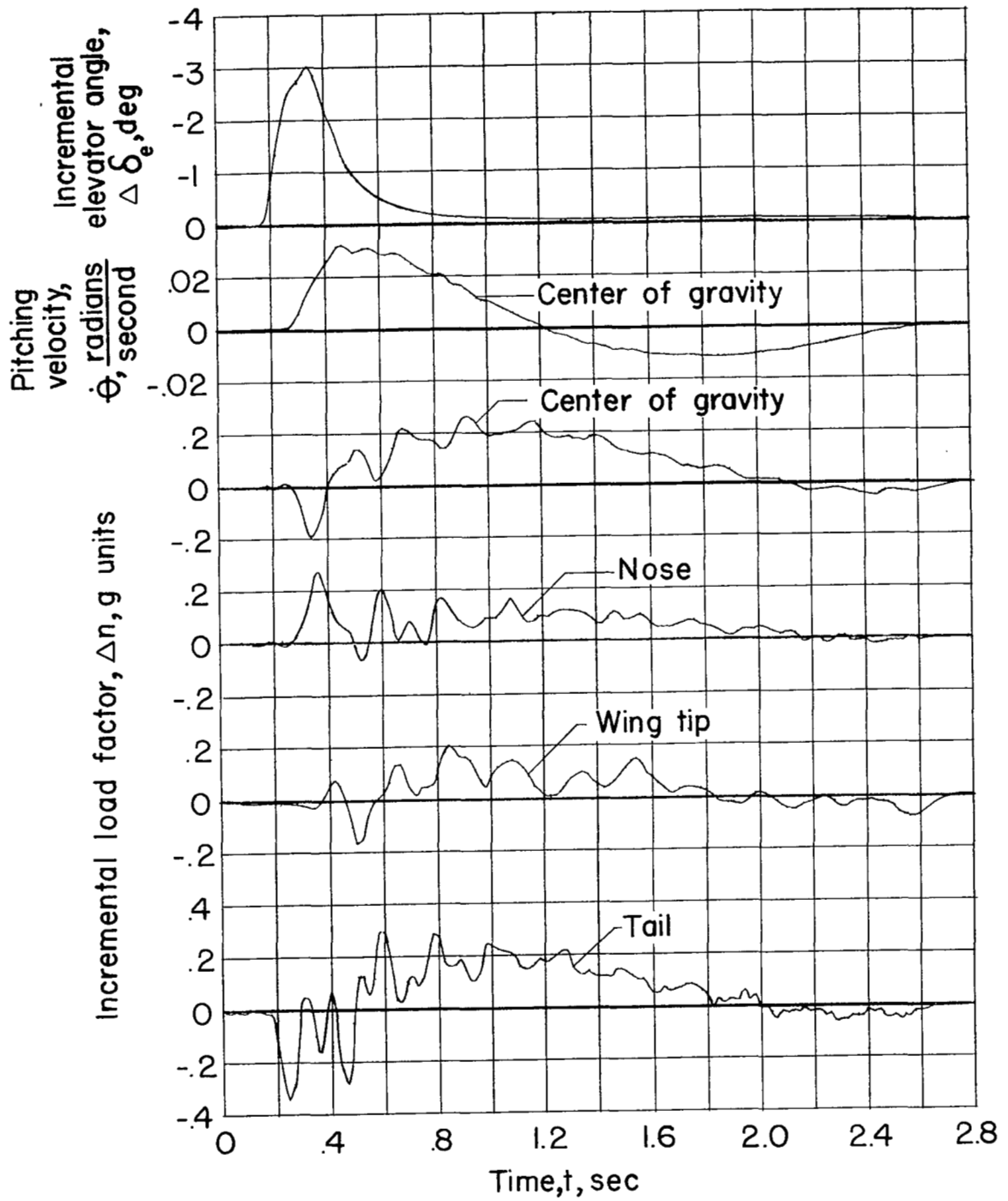
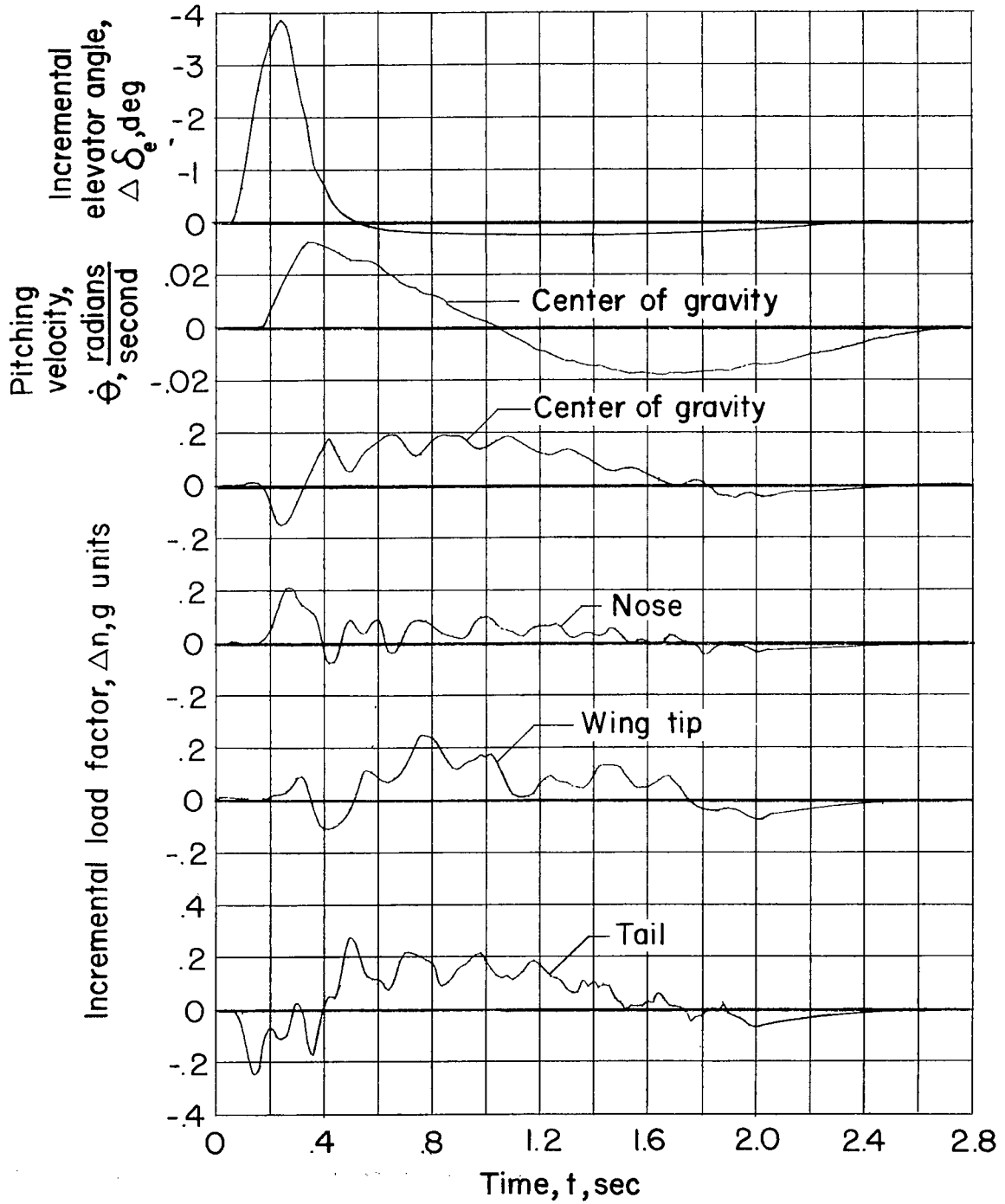
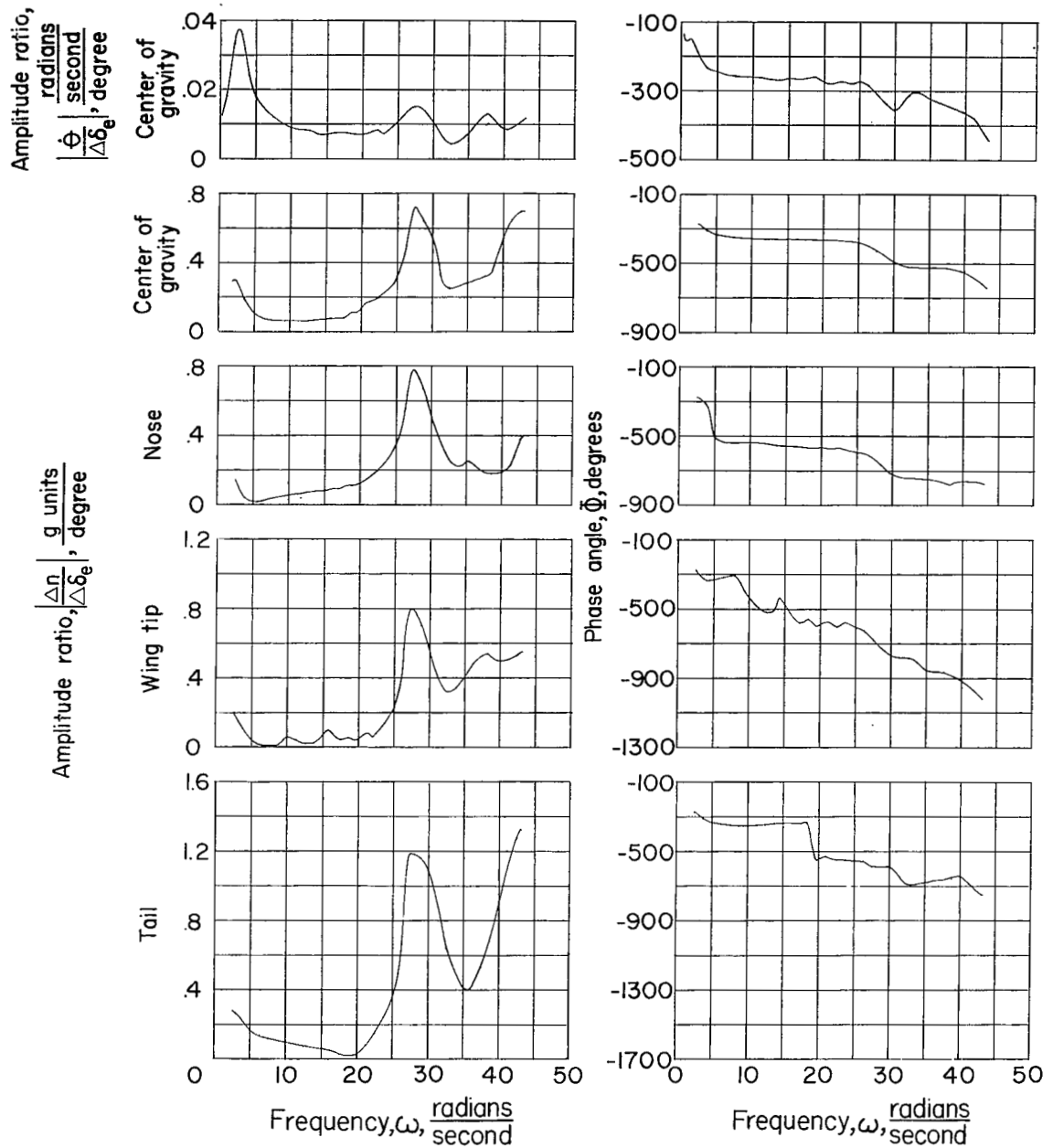
(b) $M = 0.73$.

Figure 3.- Continued.



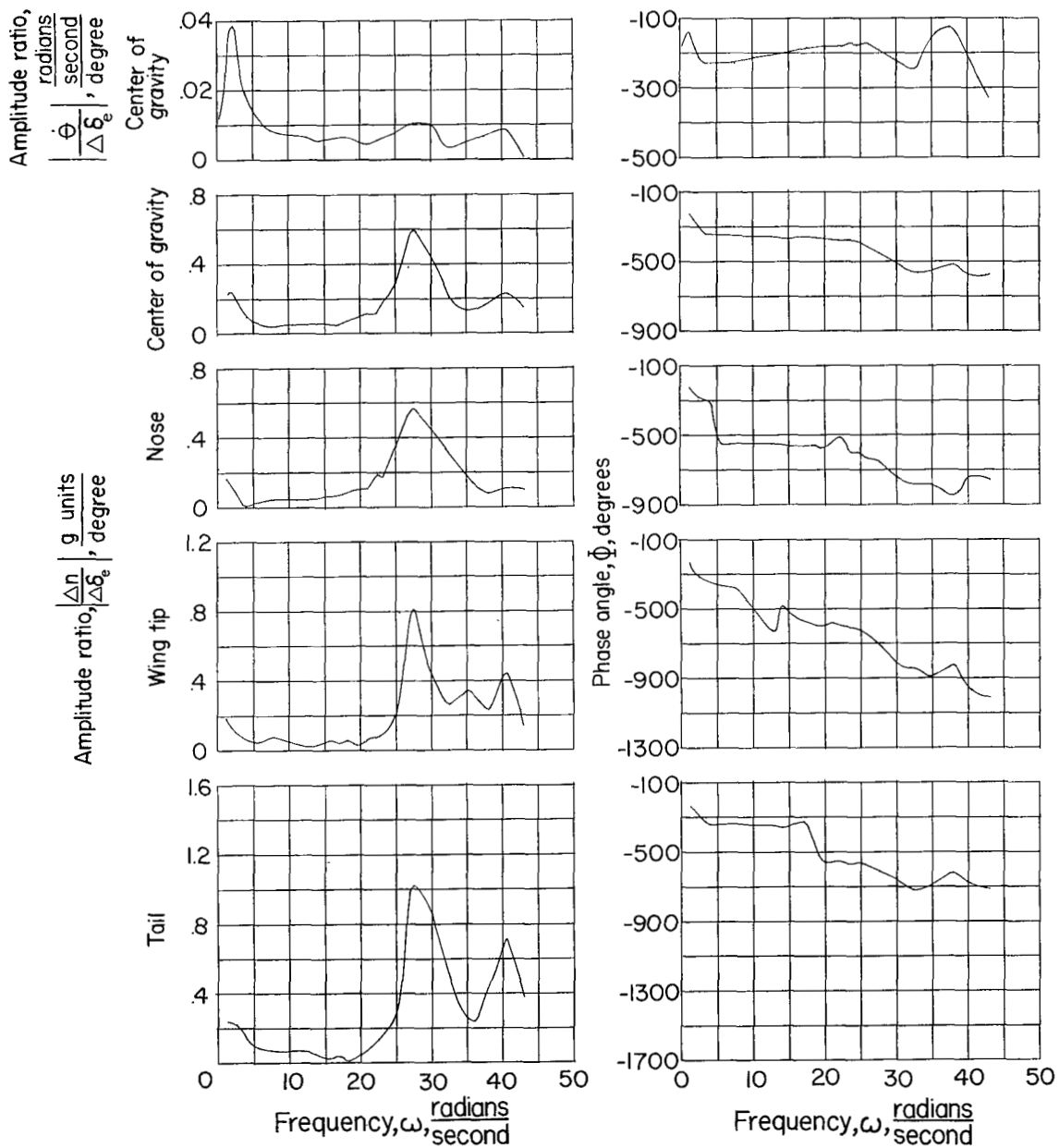
(c) $M = 0.66$.

Figure 3.- Concluded.



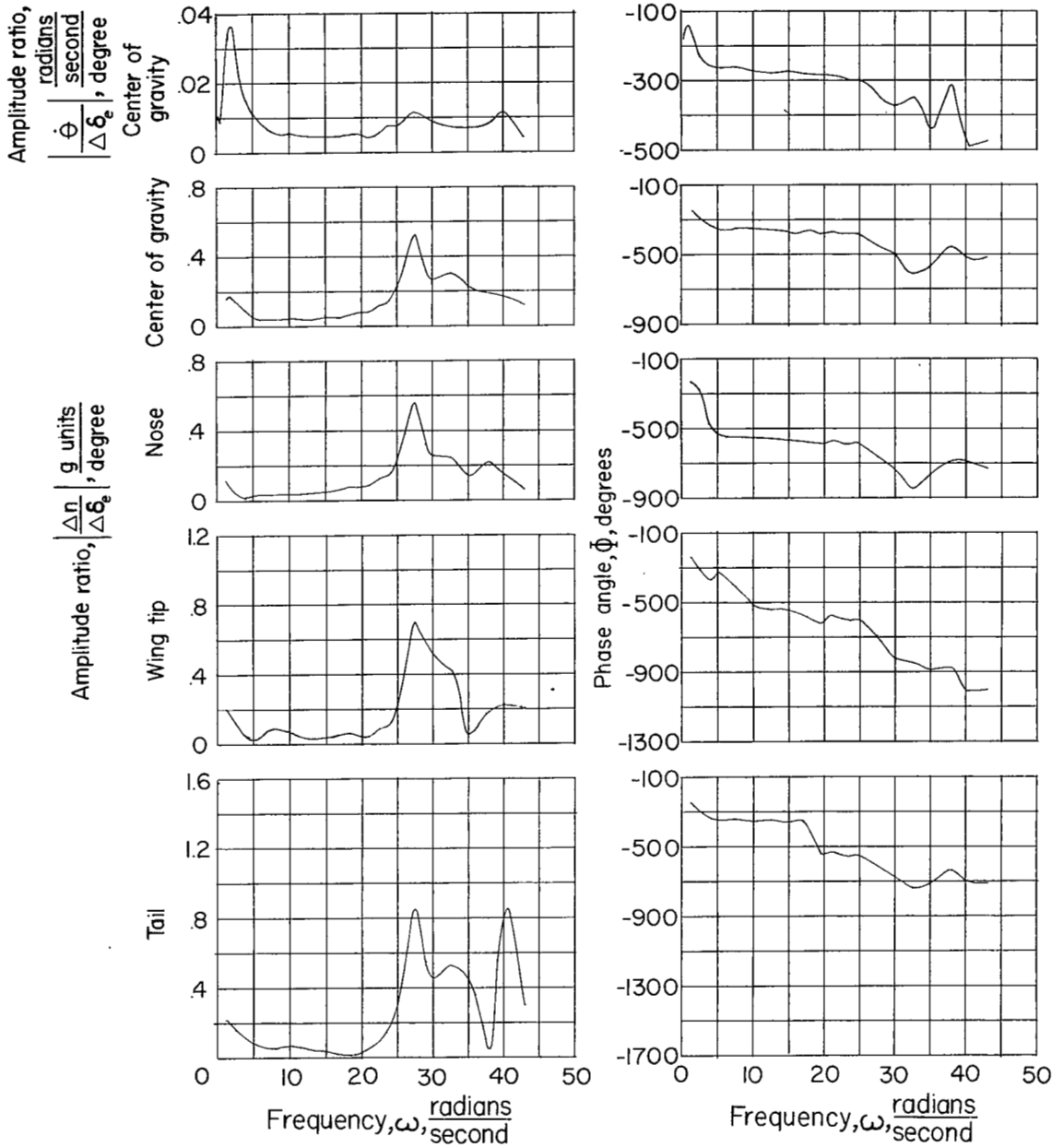
(a) $M = 0.82$.

Figure 4.- Frequency responses of measured quantities. $H_p = 30,000$ feet; center-of-gravity position at 0.21 \bar{c} .



(b) $M = 0.73$.

Figure 4.- Continued.



(c) M = 0.66.

Figure 4.- Concluded.

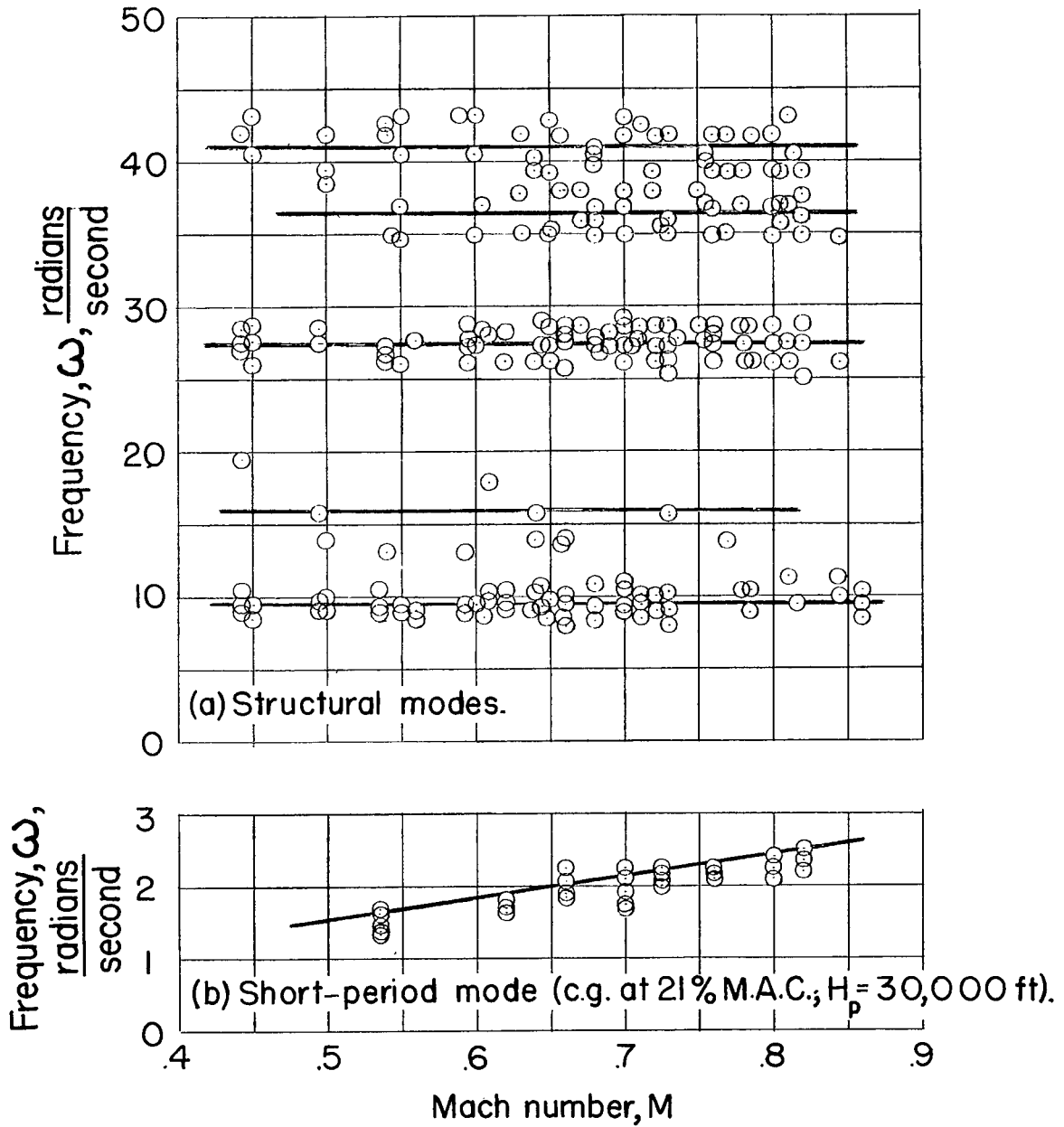


Figure 5.- Predominant symmetrical airplane frequencies.

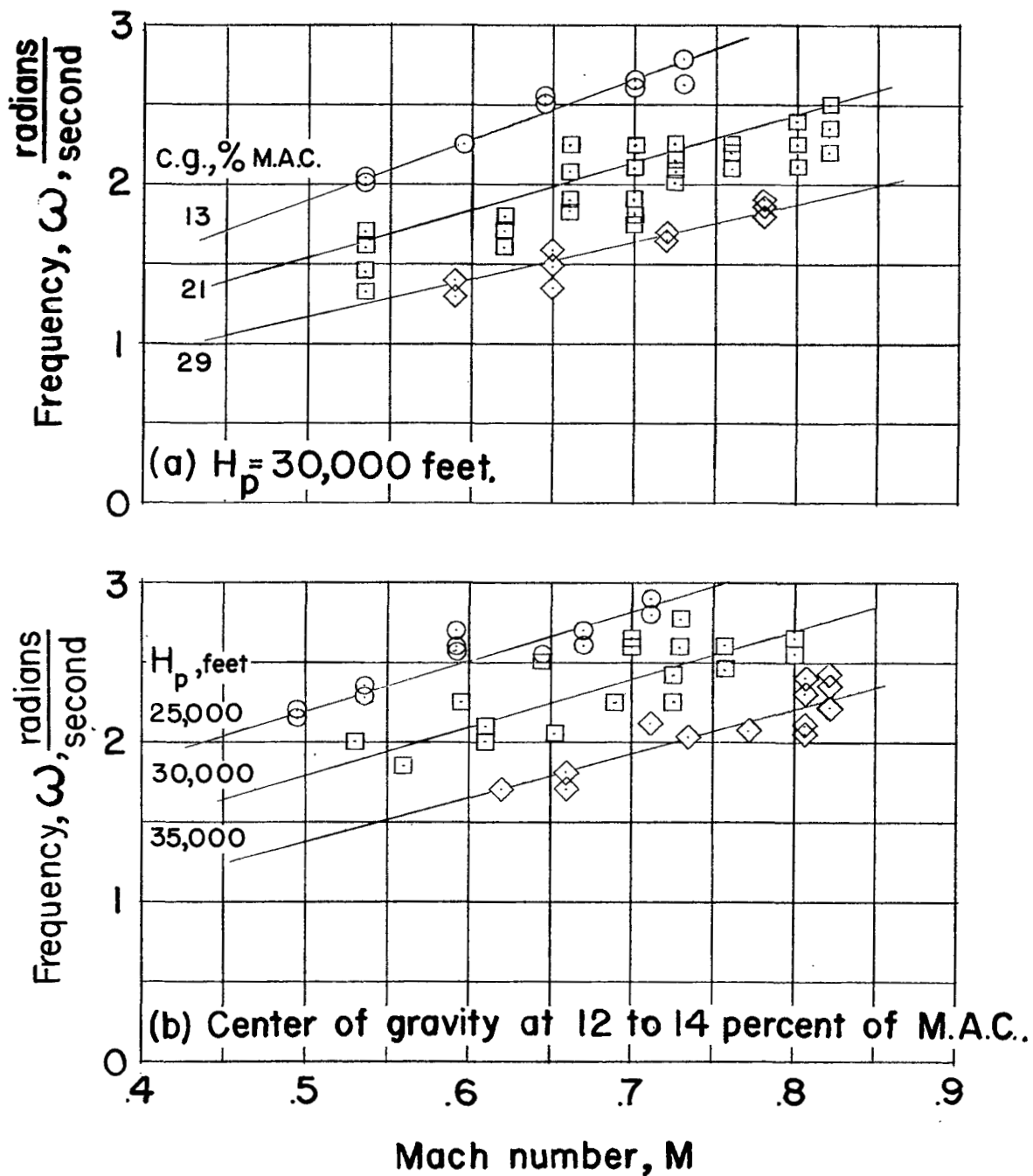


Figure 6.- Effect of altitude and center-of-gravity position on short-period natural frequency of test airplane.

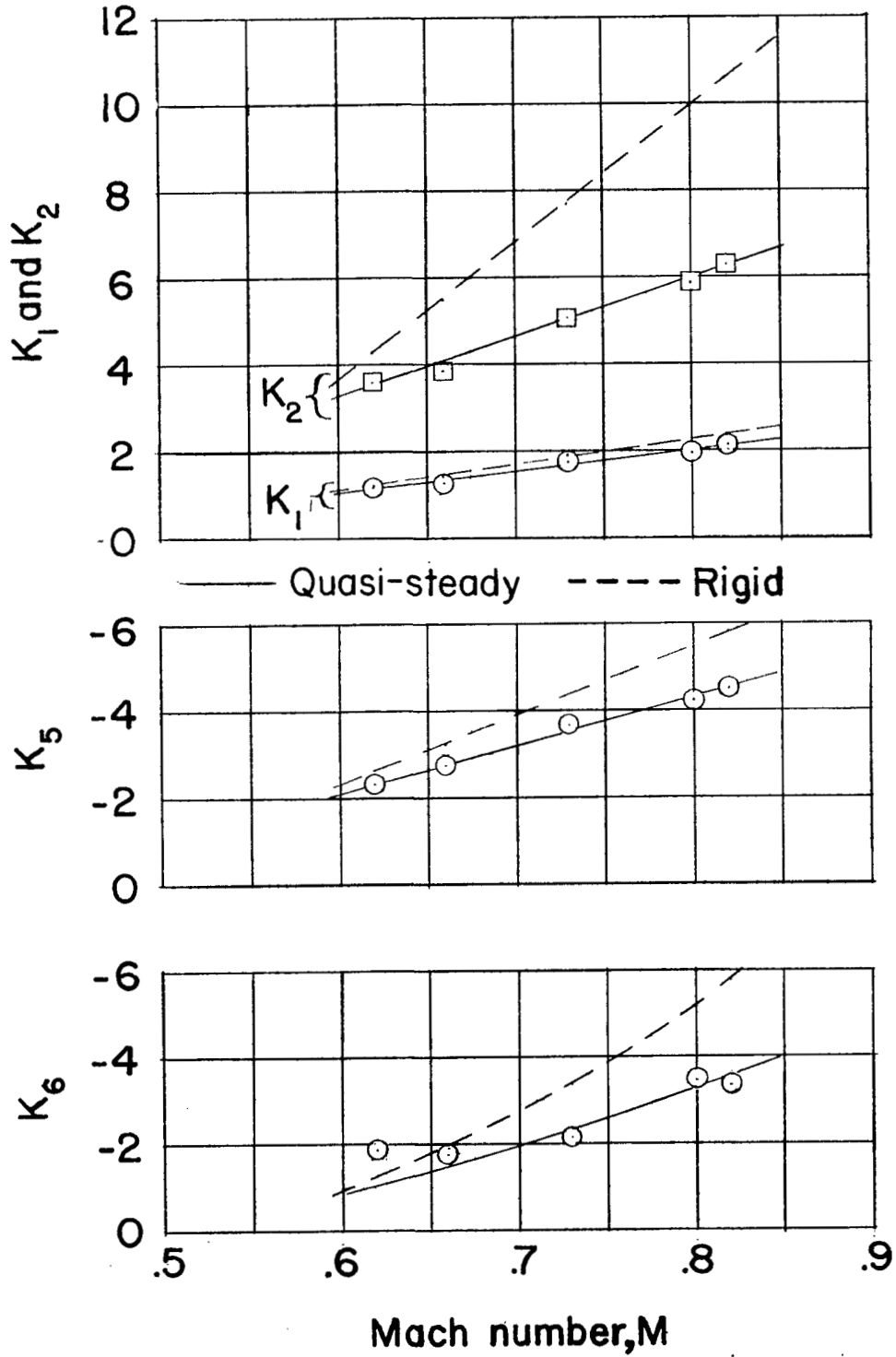
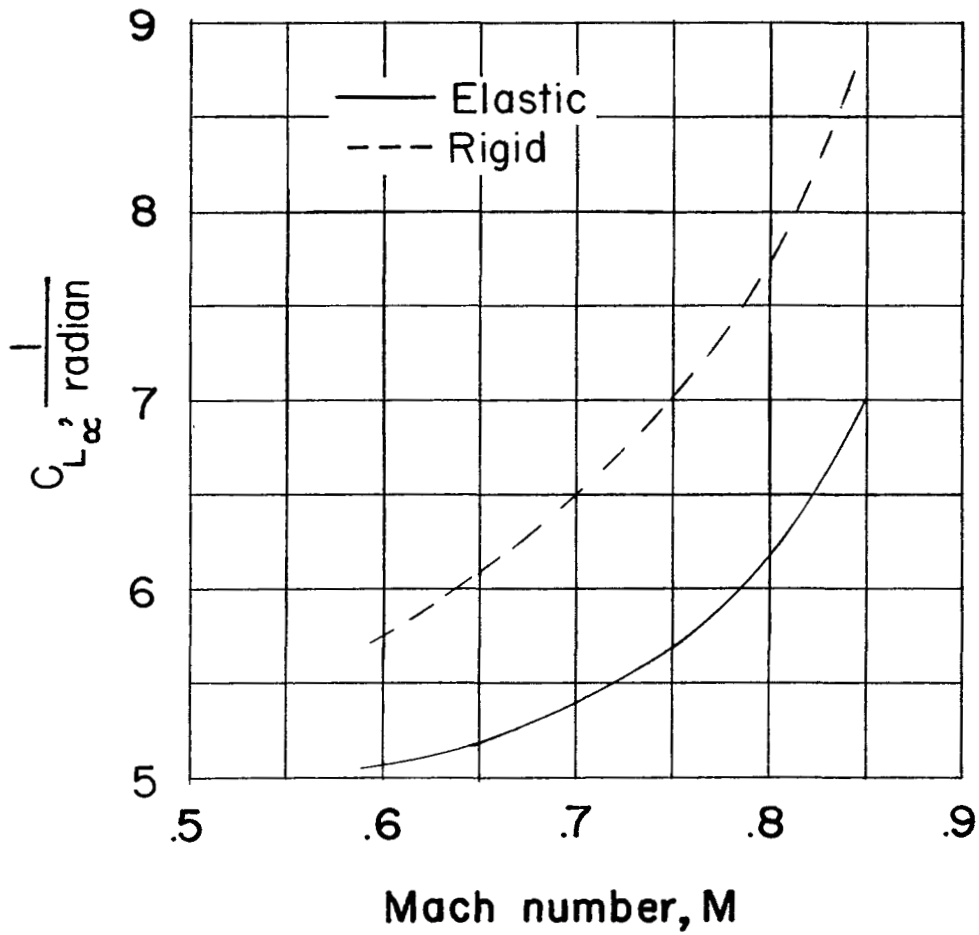
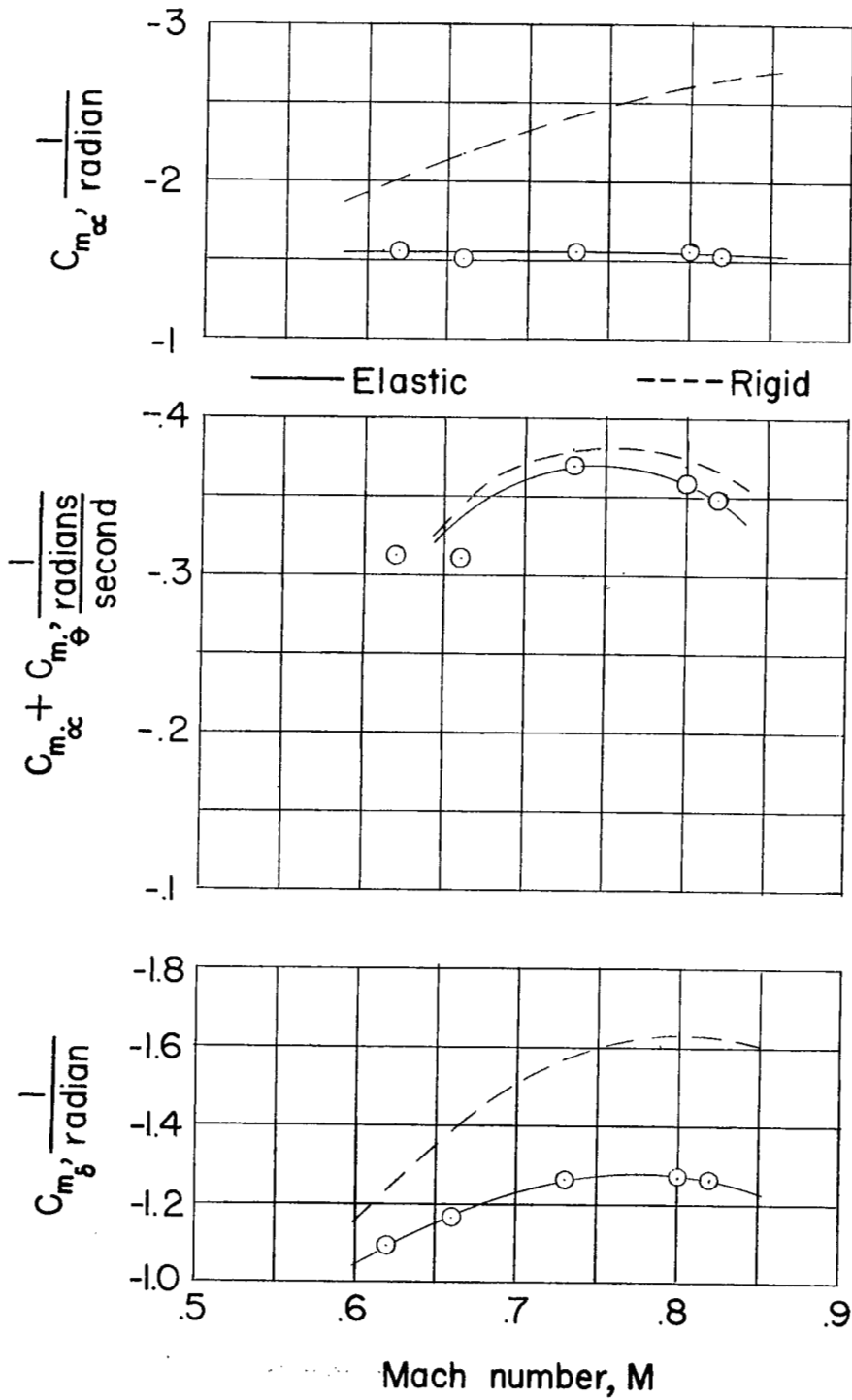


Figure 7.- Variation of pitching-velocity transfer coefficient with Mach number for test airplane. $H_p = 30,000$ feet; center-of-gravity position at $0.21\bar{c}$.



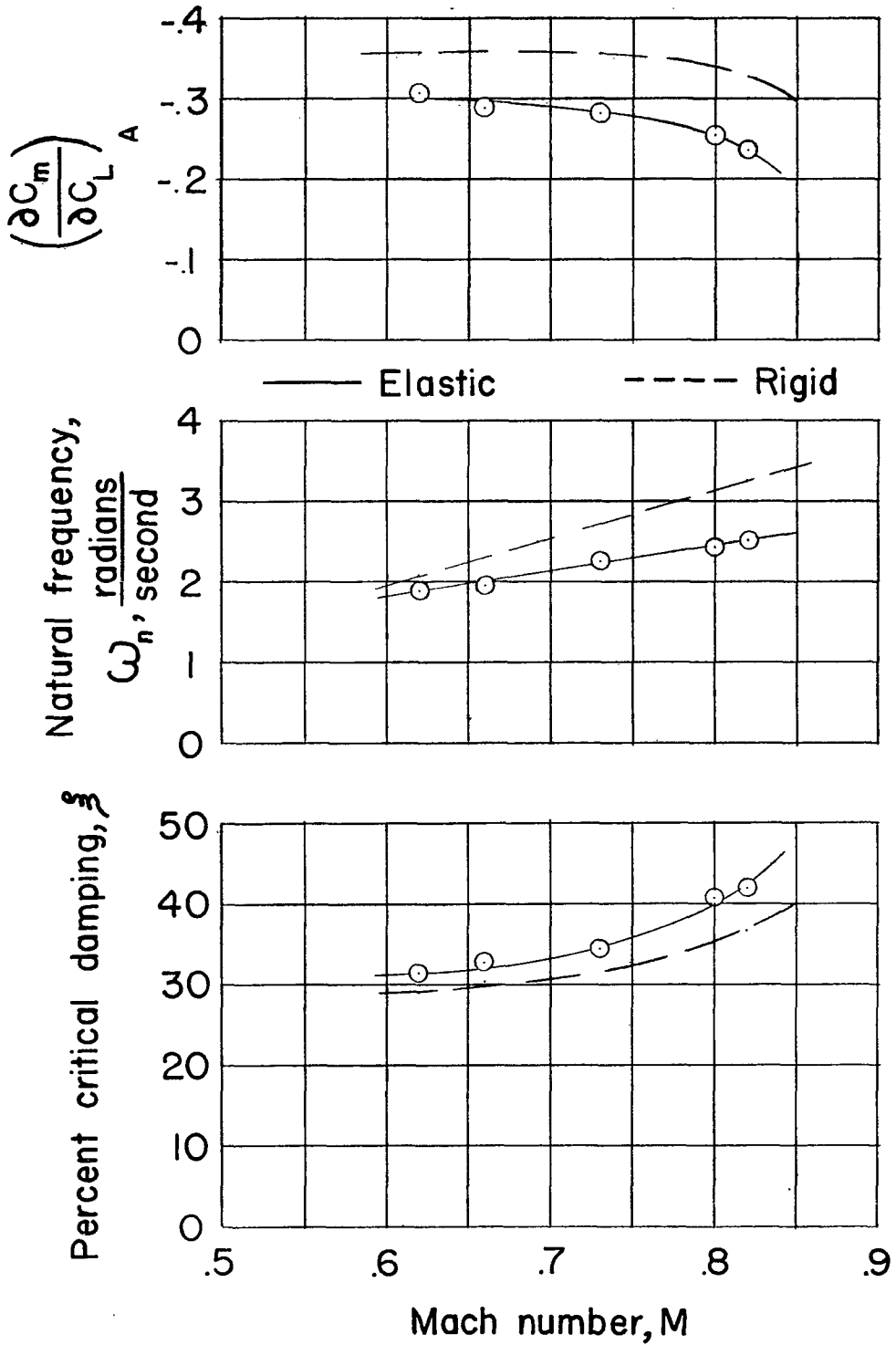
(a) Force derivatives.

Figure 8.- Variation of stability derivatives with Mach number for test airplane. $H_p = 30,000$ feet; center-of-gravity position at $0.21\bar{c}$.



(b) Moment derivatives.

Figure 8.- Continued.



(c) Other parameters.

Figure 8.- Concluded.

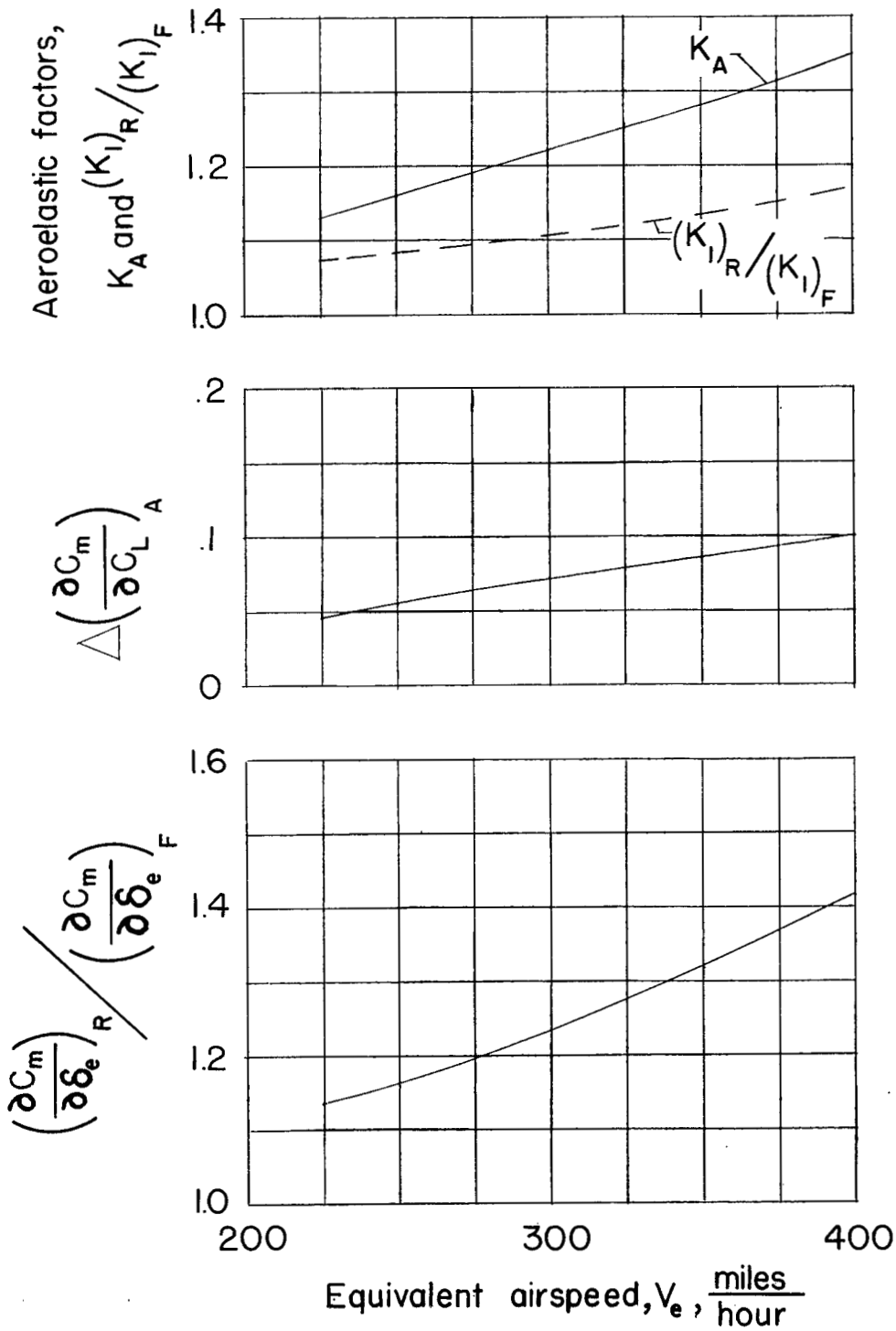


Figure 9.- Parameters used for transforming derivatives of elastic airplane to those of rigid airplane obtained from references 7 and 8 for gross weight of 125,000 pounds.

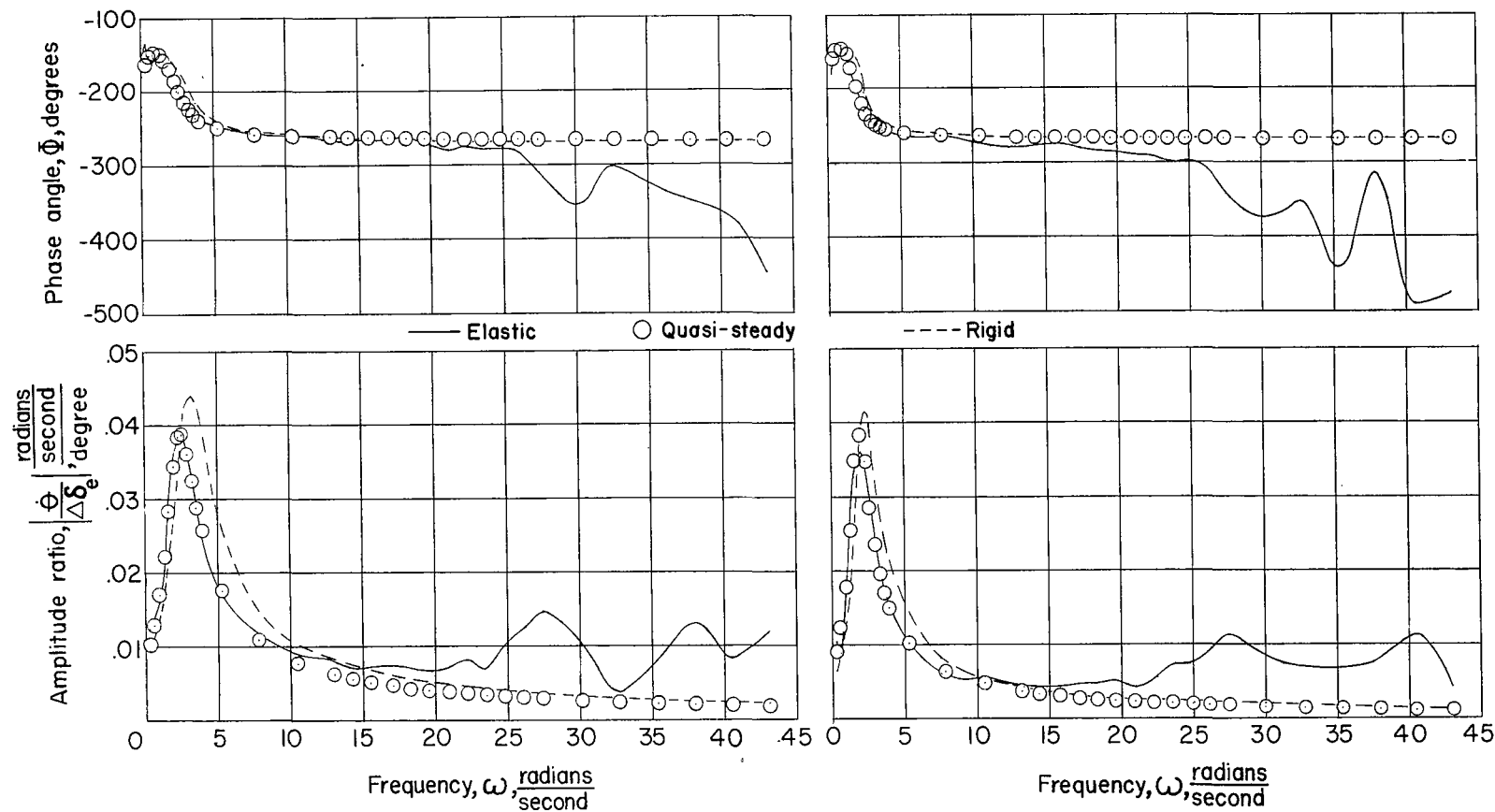
(a) $M = 0.82$.(b) $M = 0.66$.

Figure 10.- Comparison of typical elastic, quasi-steady, and rigid pitching-velocity frequency responses. $H_p = 30,000$ feet, center-of-gravity position at $0.21\bar{c}$.

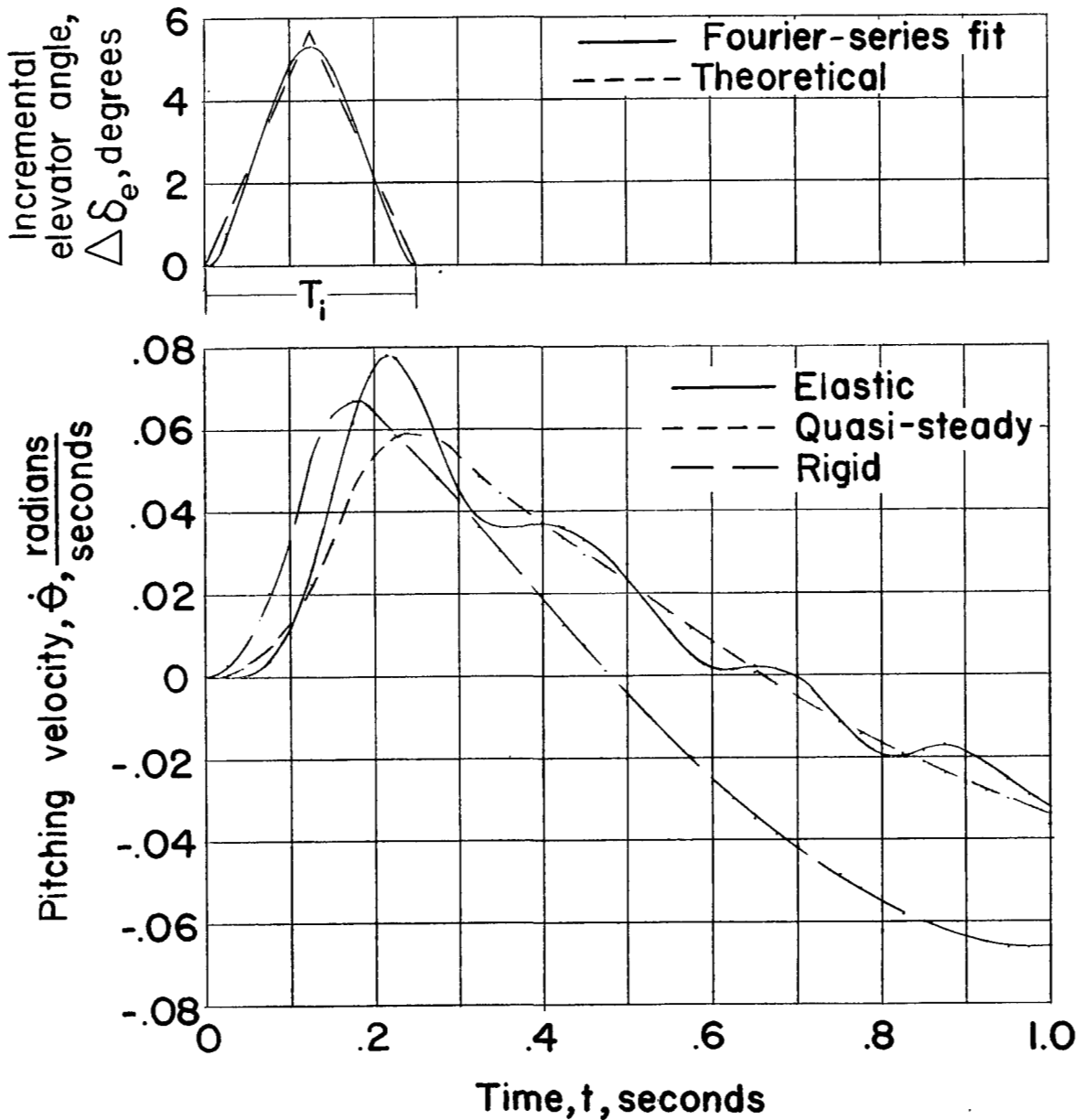


Figure 11.- Typical pitching-velocity time-history responses to frequency responses of elastic, quasi-steady, and rigid configurations due to triangular-elevator-pulse input. $T_1/T = 0.1$; $M = 0.82$; $H_p = 30,000$ feet; center-of-gravity position at $0.21\bar{c}$.

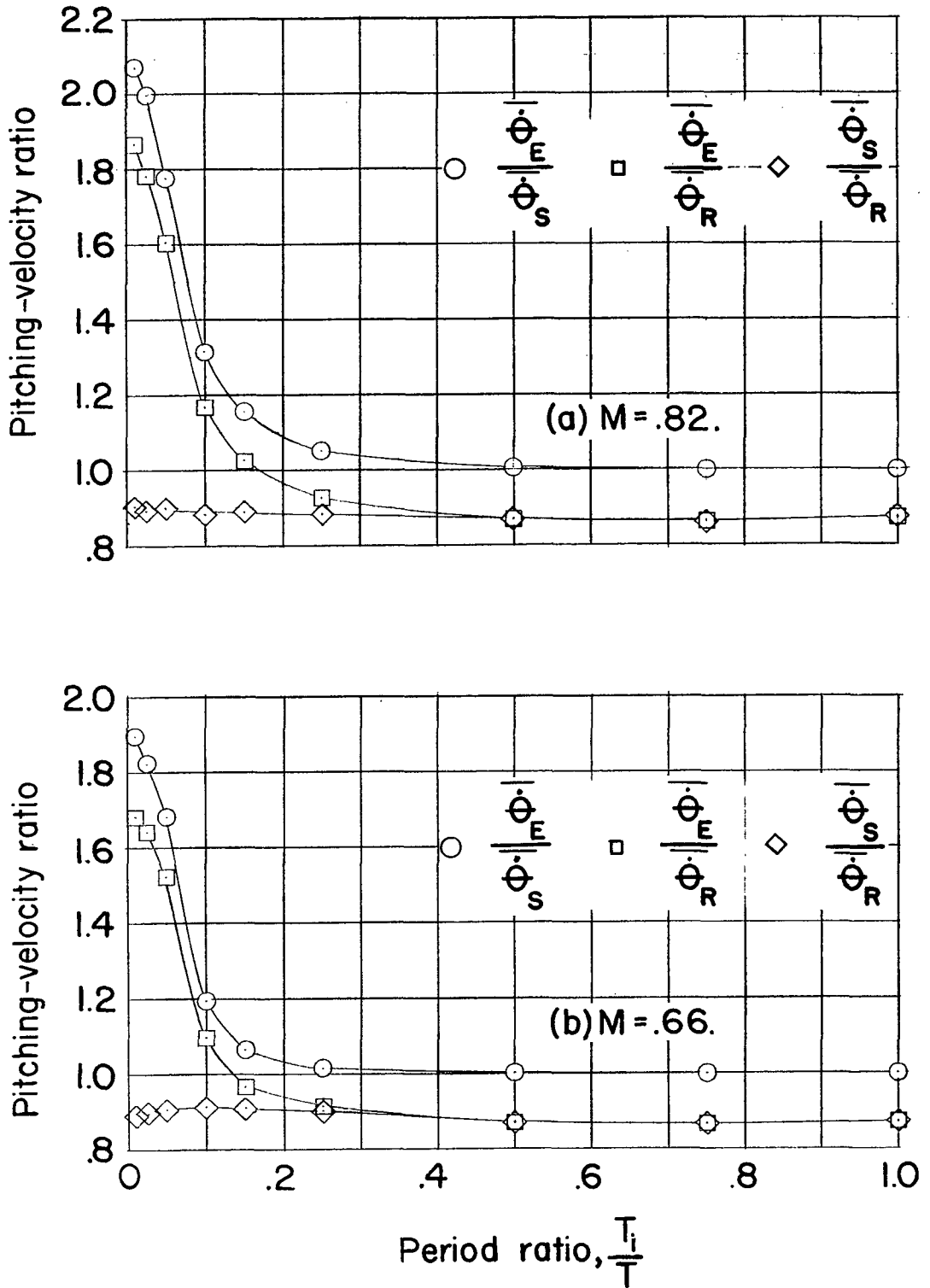


Figure 12.- Variation of ratios of maximum pitching-velocity responses with period ratio.

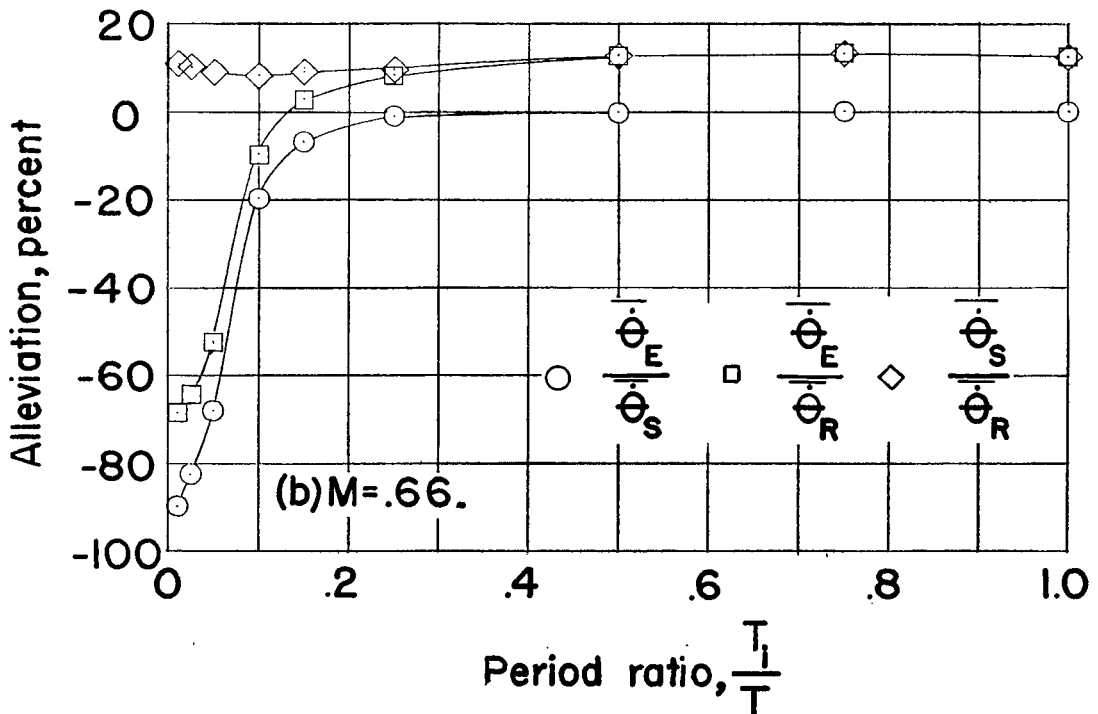
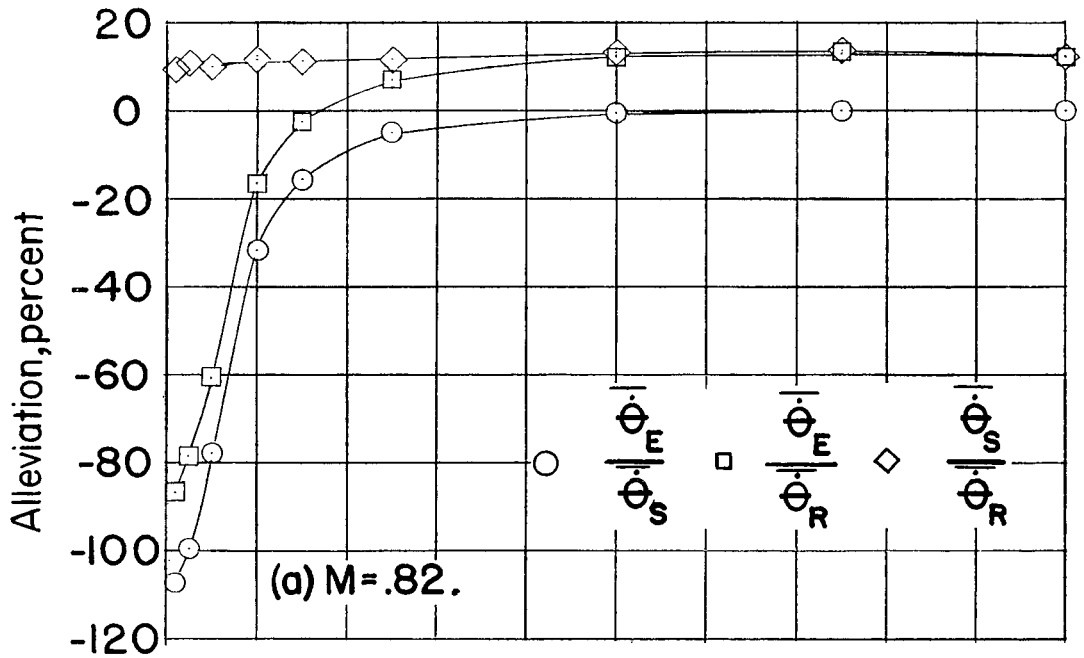
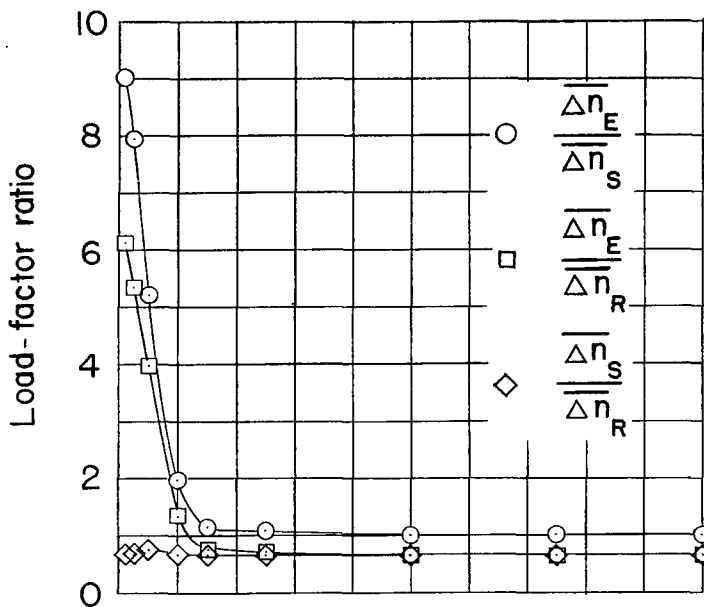
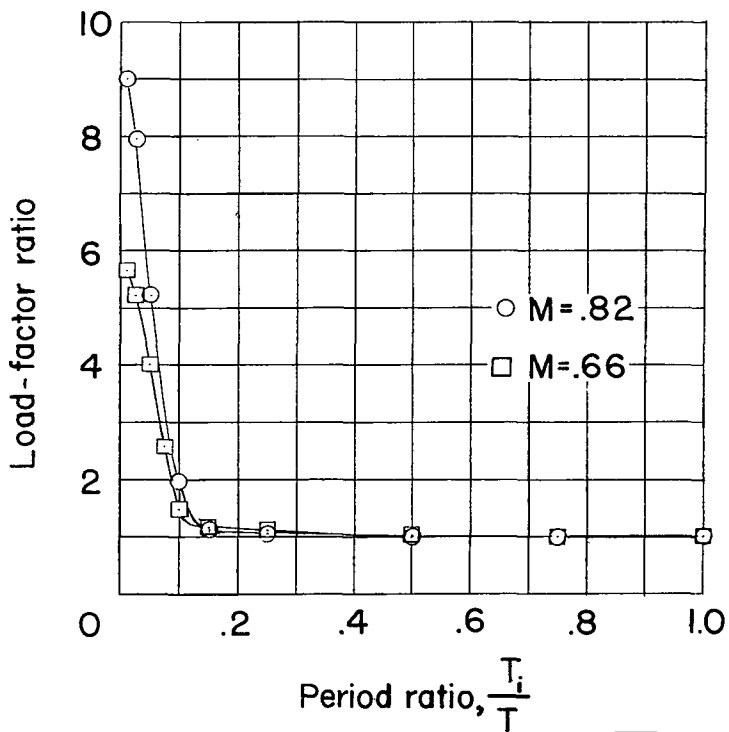


Figure 13.- Percent alleviation in pitching velocity due to effects of flexibility.



(a) Incremental load factor ratios at M=.82.



(b) Incremental load-factor ratio, $\frac{\Delta n_E}{\Delta n_S}$, at two Mach numbers.

Figure 14.- Variation of ratios of maximum incremental normal load factor with period ratio.

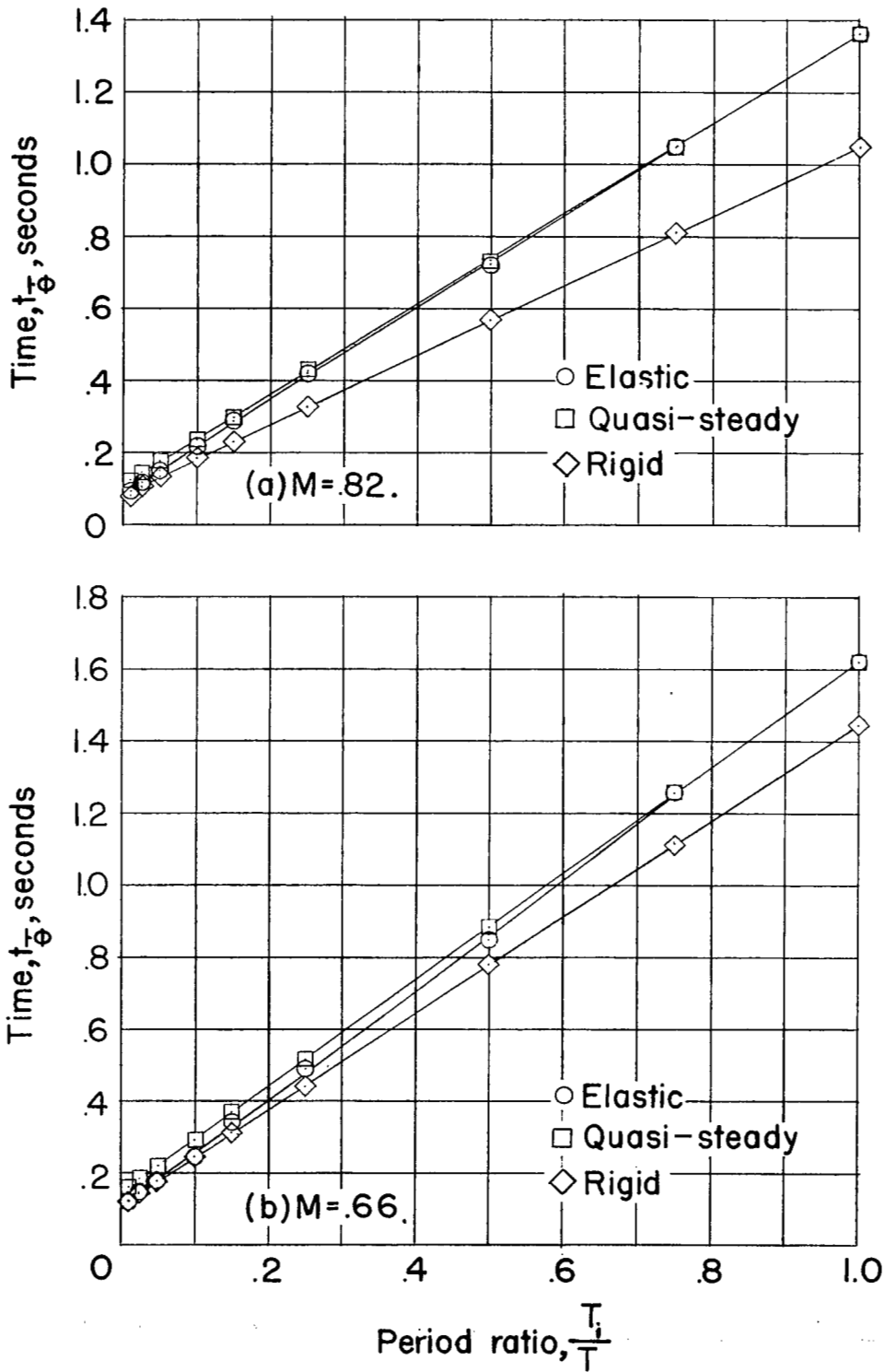


Figure 15.- Variation of time to reach peak pitching velocity with period ratio.

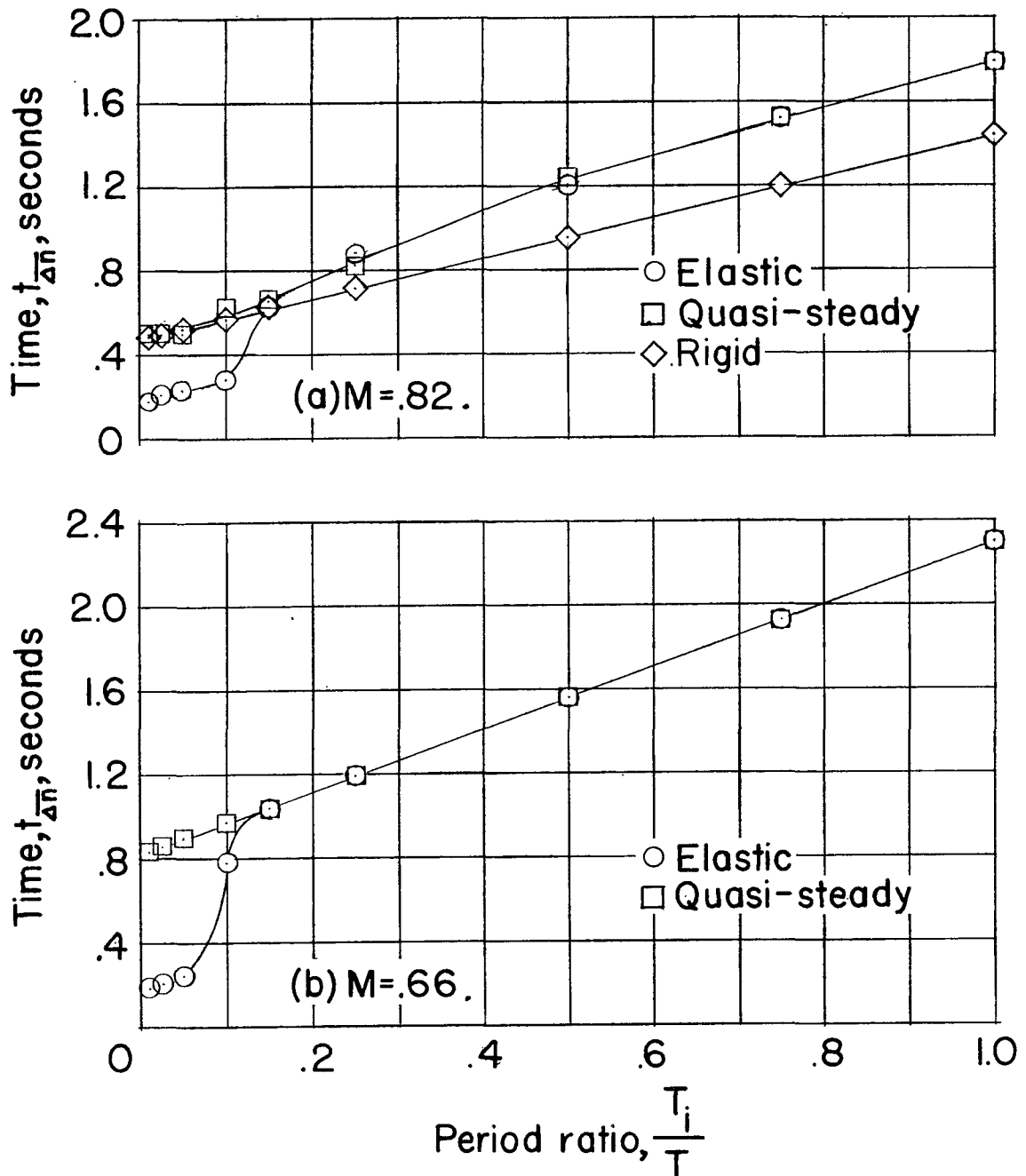


Figure 16.- Variation of time to reach the peak incremental normal load factor with period ratio.

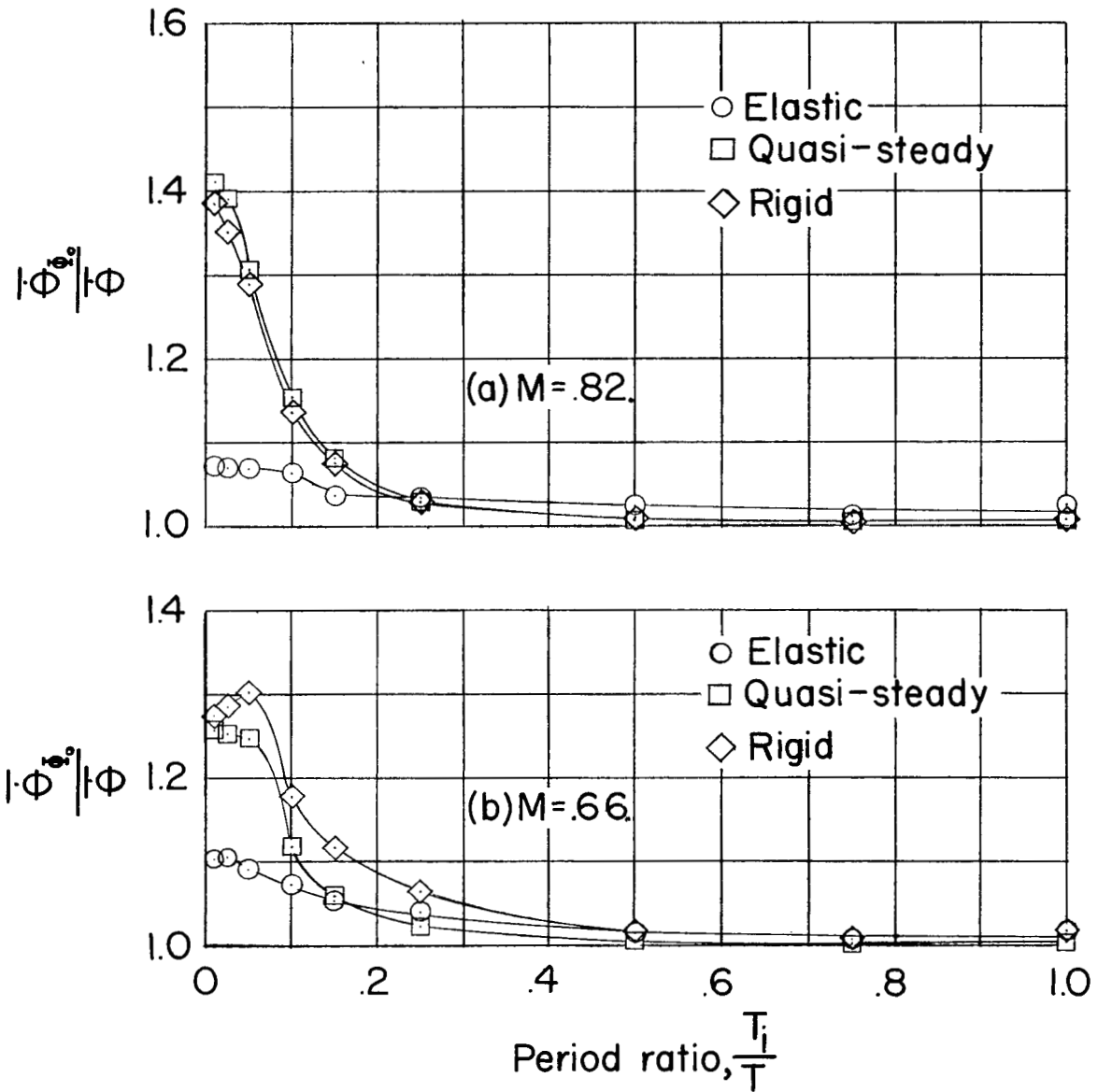


Figure 17.- Variation of ratio of maximum pitching velocity not including phasing $\dot{\Phi}_{\theta=0}$ to maximum pitching velocity including phasing $\dot{\Phi}$ with period ratio.

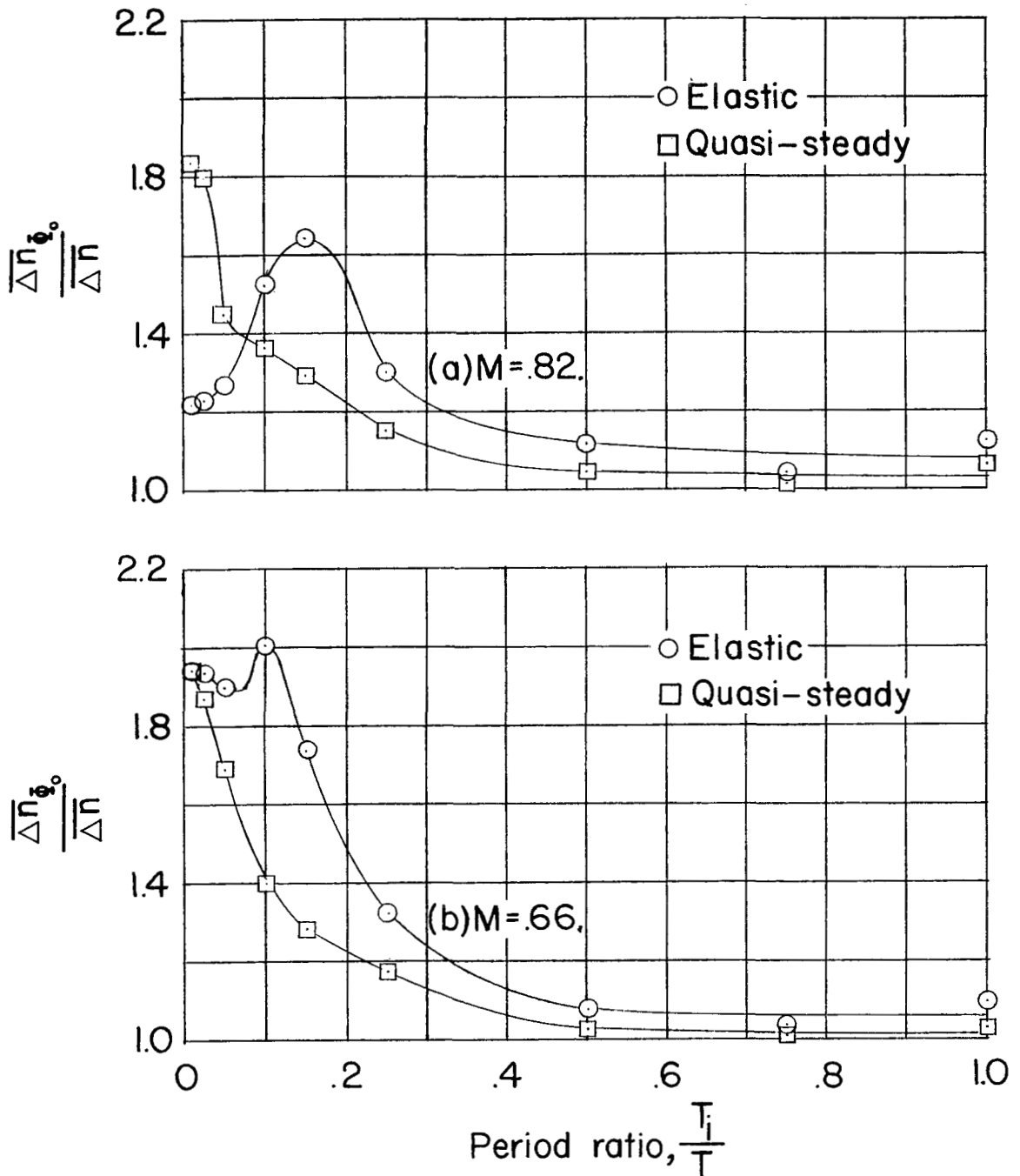
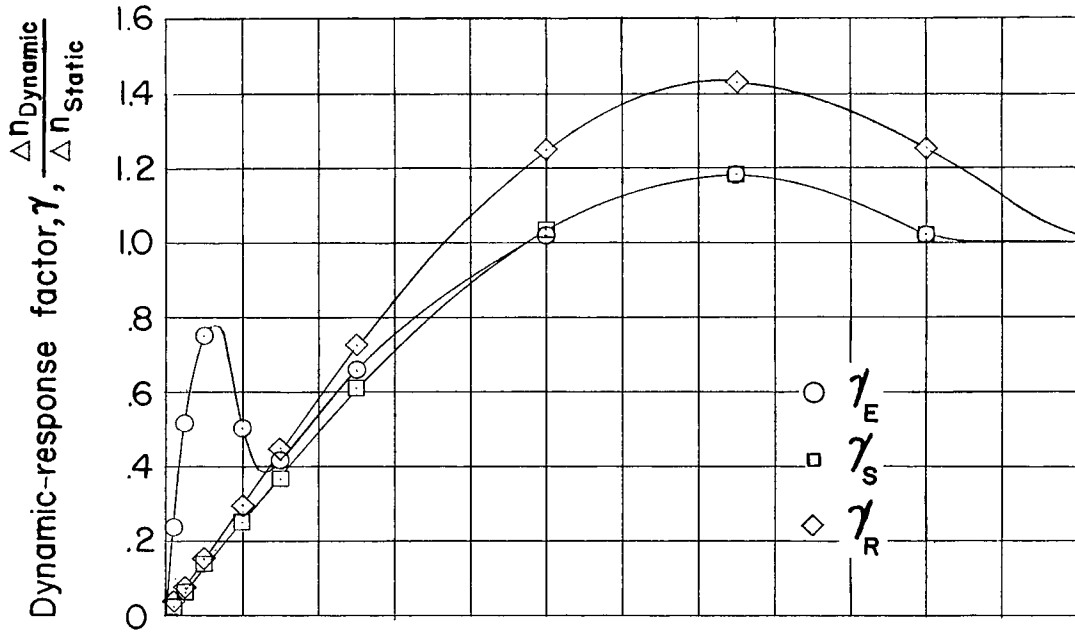
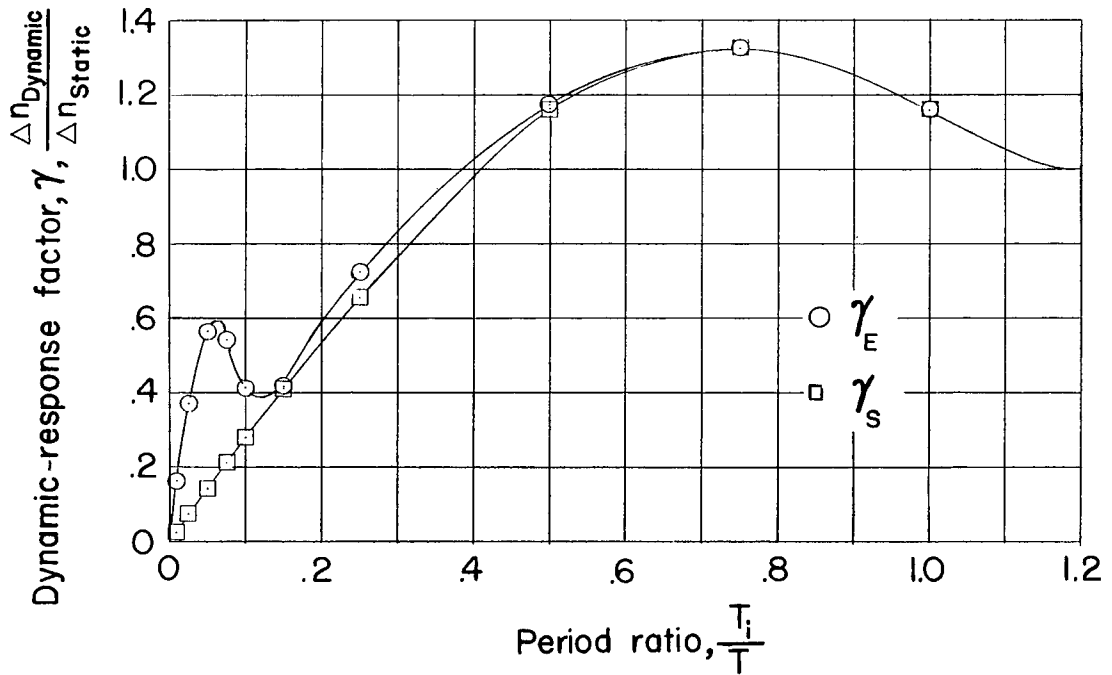


Figure 18.- Variation of ratio of maximum incremental normal load factor not including phasing $\overline{\Delta n}_{\phi=0}$ to maximum incremental normal load factor including phasing $\overline{\Delta n}$ with period ratio.



(a) $M = 0.82$ and $\Delta n_{\text{static}} = 1.30$.



(b) $M = 0.66$ and $\Delta n_{\text{static}} = 0.64$.

Figure 19.- Variation of dynamic-response factor γ with period ratio.

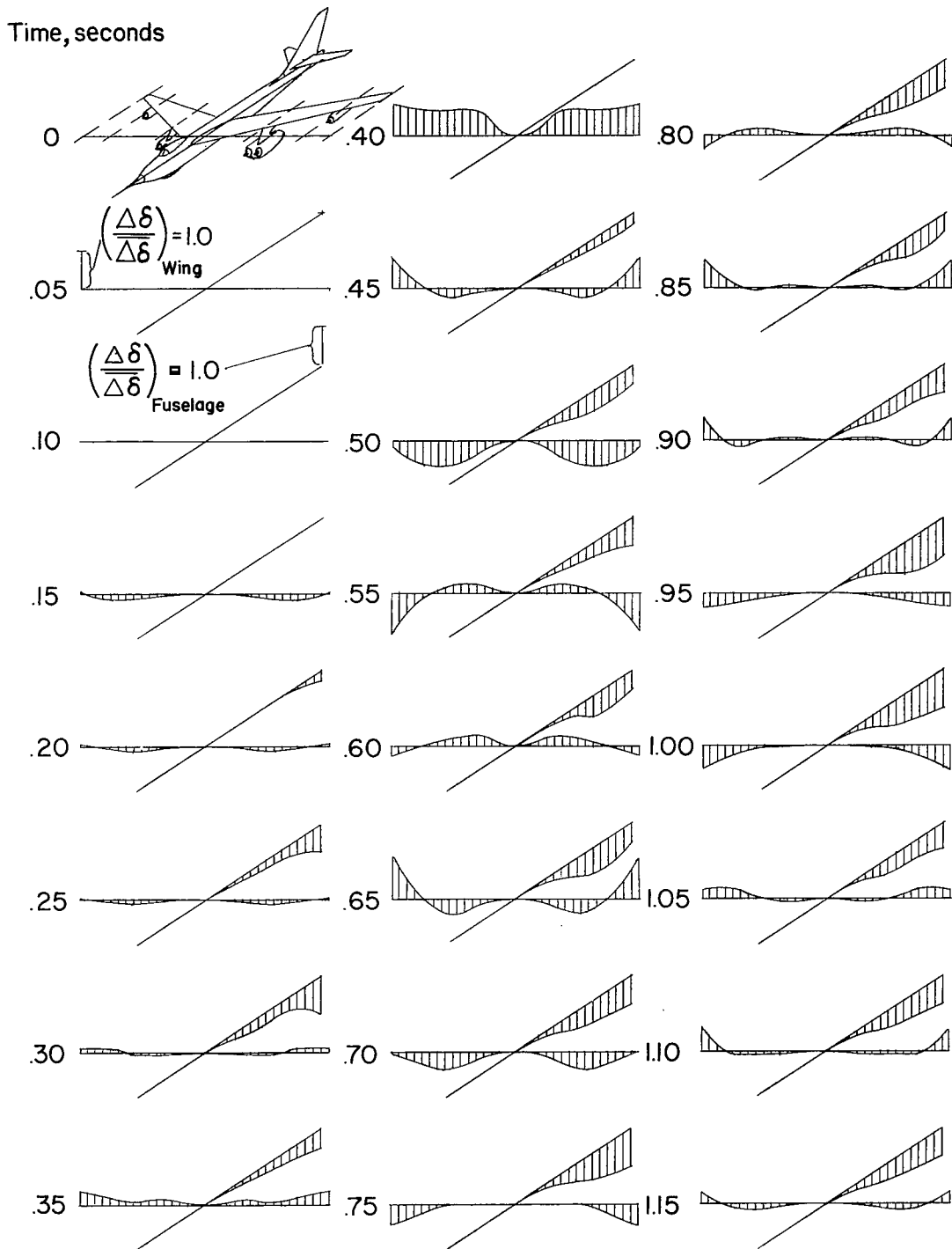


Figure 20.- Three-dimensional time histories of incremental deflections of wing and fuselage relative to center of gravity. $H_p = 30,000$ feet; center-of-gravity position at $0.21\bar{l}$; $M = 0.82$; $\overline{\Delta\delta}_{\text{wing}} = 6.0$ inches; $\overline{\Delta\delta}_{\text{fuselage}} = 1.25$ inches.

Time, seconds

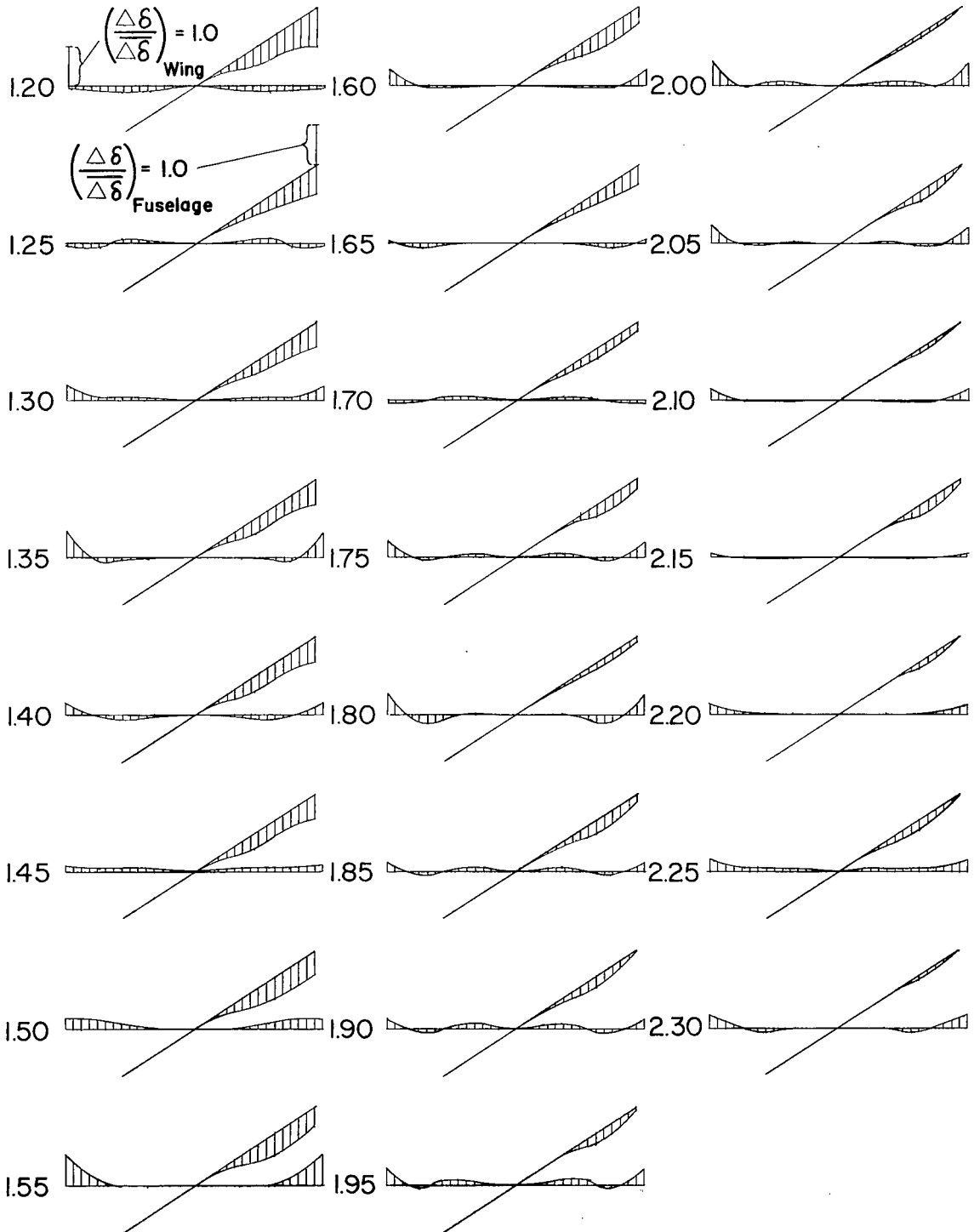


Figure 20.- Concluded.

~~CONFIDENTIAL~~

NASA Technical Library



3 1176 01437 1877

~~CONFIDENTIAL~~